Article

SOURCE DATA | TRANSPARENT PROCESS

THE EMBO JOURNAL

Transient exposure to miR-203 enhances the differentiation capacity of established pluripotent stem cells

María Salazar-Roa[1,*,†], Marianna Trakala[1,†], Mónica Álvarez-Fernández[1,†], Fátima Valdés-Mora[2,3,†], Cuiqing Zhong[4,†], Jaime Muñoz[5], Yang Yu[4], Timothy J Peters[2], Osvaldo Graña-Castro[6], Rosa Serrano[7], Elisabet Zapatero-Solana[1], María Abad[8], María José Bueno[1], Marta Gómez de Cedrón[1], José Fernández-Piqueras[9,10,11], Manuel Serrano[8,12,13], María A Blasco[7], Da-Zhi Wang[14], Susan J Clark[2,3], Juan Carlos Izpisua-Belmonte[4], Sagrario Ortega[5] & Marcos Malumbres[1,**]

Abstract

Full differentiation potential along with self-renewal capacity is a major property of pluripotent stem cells (PSCs). However, the differentiation capacity frequently decreases during expansion of PSCs *in vitro*. We show here that transient exposure to a single microRNA, expressed at early stages during normal development, improves the differentiation capacity of already-established murine and human PSCs. Short exposure to miR-203 in PSCs (*mi*PSCs) induces a transient expression of 2C markers that later results in expanded differentiation potency to multiple lineages, as well as improved efficiency in tetraploid complementation and human–mouse interspecies chimerism assays. Mechanistically, these effects are at least partially mediated by direct repression of *de novo* DNA methyltransferases Dnmt3a and Dnmt3b, leading to transient and reversible erasure of DNA methylation. These data support the use of transient exposure to miR-203 as a versatile method to reset the epigenetic memory in PSCs, and improve their effectiveness in regenerative medicine.

Keywords differentiation; epigenetics; microRNAs; pluripotency; stem cells
Subject Categories Chromatin, Transcription & Genomics; RNA Biology; Stem Cells & Regenerative Medicine

DOI 10.15252/embj.2019104324 | Received 23 December 2019 | Revised 27 May 2020 | Accepted 28 May 2020 | Published online 2 July 2020
The EMBO Journal (2020) 39: e104324

Introduction

Pluripotent stem cells (PSCs) provide an important promise for regenerative medicine due to their self-renewal potential and ability to differentiate into multiple cell lineages. During the last years, multiple efforts have been put into improving the potential of these cells either by expanding their differentiation capacity into a wider variety of cell lineages or by improving maturation properties into specific functional cell types (Li & Izpisua Belmonte, 2016; Takahashi & Yamanaka, 2016). PSCs are commonly cultured in the presence of Mek1/2 and Gsk3 inhibitors together with the cytokine Lif (2i/L conditions Ying *et al*, 2008). Although these conditions may improve the maintenance of pluripotency *in vitro*, recent evidences suggest that prolonged inhibition of Mek1/2 may limit the developmental and differentiation capacity of PSCs *in vivo*, in part by inducing irreversible demethylation of imprinting control regions (ICRs) (Choi *et al*, 2017a; Yagi *et al*, 2017). Recent data suggest that genetic ablation of miR-34 in PSCs results in improved potential to

1 Cell Division and Cancer Group, Spanish National Cancer Research Centre (CNIO), Madrid, Spain
2 Epigenetics Research Program, Genomics and Epigenetics Division, Garvan Institute of Medical Research, Sydney, NSW, Australia
3 St. Vincent's Clinical School, UNSW, Sydney, Sydney, NSW, Australia
4 Gene Expression Laboratory, The Salk Institute for Biological Studies, La Jolla, CA, USA
5 Transgenics Unit, CNIO, Madrid, Spain
6 Bioinformatics Unit, CNIO, Madrid, Spain
7 Telomeres and Telomerase Group, CNIO, Madrid, Spain
8 Tumor Suppression Group, CNIO, Madrid, Spain
9 Centro de Biología Molecular Severo Ochoa (CBMSO), Consejo Superior de Investigaciones Científicas-Universidad Autónoma de Madrid (CSIC-UAM), Madrid, Spain
10 Centro de Investigación Biomédica en Red para Enfermedades Raras (CIBERER), Instituto de Salud Carlos III, Madrid, Spain
11 Instituto de Investigación Biosanitaria, Fundación Jimenez Díaz, Madrid, Spain
12 Institute for Research in Biomedicine (IRB Barcelona), The Barcelona Institute of Science and Technology (BIST), Barcelona, Spain
13 Catalan Institution for Research and Advanced Studies (ICREA), Barcelona, Spain
14 Cardiovascular Research Division, Boston Children's Hospital, Harvard Medical School, Boston, MA, USA
*Corresponding author. Tel: +34 917 328 000; ext 3452; E-mail: msalazar@cnio.es
**Corresponding author. Tel: +34 917 328 000; ext 3450; E-mail: malumbres@cnio.es
†These authors contributed equally to this work

form embryonic and extraembryonic tissues in part by promoting Gata2 expression (Choi *et al*, 2017b), although the conditions for applying this information to favor the differentiation potential of PSCs remain to be established. Finally, a recent alternative proposal suggests the use of a chemical cocktail of inhibitors that also enhances the developmental potential of PSCs (Yang *et al*, 2017); however, the applicability of this method is still limited due to the lack of mechanistic details.

Here, we identified miR-203 as a microRNA preferentially expressed in the 2C-morula stages during pre-implantation development in the mouse embryo. By using a variety of *in vitro* and *in vivo* approaches, we report that transient exposure of already-established induced pluripotent stem cells (iPSCs) or ESCs to miR-203 enhances the ability of these PSCs to differentiate into multiple cell lineages and to reach further maturation properties. Transient expression of miR-203 in PSCs (*mi*PSCs) leads to greater developmental potential in tetraploid complementation assays, and significantly improves the efficiency of human iPSCs in contributing to interspecies human–mouse conceptuses. Mechanistically, these effects are at least partially mediated through the miR-203-dependent control of *de novo* DNA methyltransferases Dnmt3a and Dnmt3b, thereby regulating the DNA methylation landscape of these *mi*PSCs. These observations suggest that the developmental and differentiation potential of already-established PSCs can be readily enhanced by transient exposure to a single microRNA.

Results

miR-203 improves the differentiation potency of PSCs

miR-203 was originally proposed to limit the stemness potential of skin progenitors (Yi *et al*, 2008) and to display tumor-suppressive functions in multiple cancers (Bueno *et al*, 2008; Michel & Malumbres, 2013), suggesting a role in the balance between stemness and differentiation. However, its expression during early development remained undefined. A first analysis of miR-203 levels during normal murine and bovine development suggested a modest but specific wave of expression during early development (blastocyst stage in murine and more particularly hatched blastocysts in bovine embryos), whereas its expression was lost in cultured embryonic stem cells (Yang *et al*, 2008; Goossens *et al*, 2013). Interestingly, our quantitative PCR analysis in mouse embryos isolated at different early developmental stages showed that miR-203 expression was low in oocytes, slightly induced at the 2-cell stage, and displayed a gradual reduction in morulas and blastocysts (Fig 1A).

To easily manipulating miR-203 levels *in vitro* and *in vivo*, we generated a tetracycline-inducible knock-in model in which the miR-203-encoding sequence was inserted downstream of the type I collagen gene and expressed under the control of a tetracycline-responsive element [*ColA1*(miR-203) allele] in the presence of tetracycline reverse transactivator expressed from the *Rosa26* locus [*Rosa26*(rtTA) allele] (Fig EV1A). Treatment of *ColA1*(miR-203/miR-203); *Rosa26*(rtTA/rtTA) mouse embryonic fibroblasts (MEFs) or ESCs with doxycycline (Dox) led to a significant induction of miR-203 levels (Fig EV1B). We also generated iPSCs from wild-type or un-induced *ColA1*(miR-203/miR-203); *Rosa26*(rtTA/rtTA) MEFs by using lentiviral vectors expressing Oct4, Sox2, Klf4, and cMyc (Takahashi & Yamanaka, 2006). Similar to MEFs or ESCs, these mutant iPSCs showed a significant induction of miR-203 after treatment with doxycycline (Fig EV1B). Although previous reports have suggested that this system suffers of relative leakiness (Stadtfeld *et al*, 2010b), miR-203 expression significantly reduced and was undetectable a few days after Dox withdrawal (Fig EV1C).

We next studied the long-term effects of miR-203 by treating *ColA1*(miR-203/miR-203); *Rosa26*(rtTA/rtTA) iPSCs (generated in the absence of Dox) transiently with Dox for 5 days (microRNA transiently induced iPSCs or *mi*iPSCs; Fig 1B). RNA sequencing of

Figure 1. Effects of transient induction of miR-203 in iPSC and ESC pluripotency and differentiation potential.

A miR-203 expression, as determined by qPCR, in five temporal different stages of normal early development: oocyte, 2-cell embryo, morula, compacted morula, and blastocyst. RNA was extracted from 30 different embryos and pooled in two independent groups for analysis by qPCR. RNA expression is normalized by a housekeeping miRNA (miR-16) that maintained invariable during early embryogenesis. Data represent the mean of 6 different qPCR measures (red bars). $P = 0.05$ (Student's *t*-test) comparing 2C/morula versus compacted morula/blastocyst.

B Protocol for reprogramming of miR-203 mutant MEFs into pluripotent iPSCs and subsequent differentiation into embryoid bodies. MEFs were transduced with lentiviruses expressing Oct4, Sox2, Klf4, and cMyc (OSKM) in a constitutive manner. The resulting iPSCs were then treated with doxycycline (Dox) 1 μg/ml during 5 days to induce miR-203 expression. "*mi*iPSCs" refers to iPSCs in which miR-203 was transiently expressed during the indicated 5 days. Dox was removed for 15–30 days before starting the embryoid body generation protocol. Samples for RNA sequencing were taken 30 days after Dox withdrawal.

C Principal component analysis of RNAseq data from wild-type iPSCs ($n = 3$ clones), *mi*iPSCs ($n = 4$), and wild-type ESCs ($n = 3$).

D Enrichment plots of the 282-gene 2-cell signature (Biase *et al*, 2014) in *mi*iPSCs 10 and 25 days after Dox withdrawal.

E PCA of RNAseq and microarray data from *mi*iPSCs and known already-published PSC types. Log2 expression values were normalized to mESCs in each study. Data from *mi*iPSCs (this study), mES cells (each study), 2C-like cells (MacFarlan et al, 2012), and epiblast stem cells (*Najm et al, 2011*) were analyzed, and a total of 17,243 genes were selected. For *mi*iPSCs, clones 1 and 2 were analyzed 10 days after miR-203 exposure, while clones 3 and 4 were analyzed 25 days after miR-203 exposure (see schematic shown in Fig 1B). For Tomato PSCs, Tomato fluorescence is associated with 2C-like retrotransposon expression, and thus, Tomato-positive cells are identified as 2C-like cells (Macfarlan *et al*, 2012).

F Representative images of embryoid bodies (EBs) derived from wild-type iPSCs or ESCs, or from *mi*iPSC and *mi*ESCs at day 30 of differentiation. Scale bars, 500 μm.

G Quantification of the percentage of EBs from panel (F) presenting internal large cavities and EBs beating during the indicated time course. Data are represented as mean ± SEM ($n = 3$ independent experiments). $^*P < 0.05$; $^{***}P < 0.001$ (Student's *t*-test).

H Representative images of EBs derived from human iPSCs transiently transfected with either control (left) or miR-203 mimics (right), at different time points during the differentiation process. Scale bars, 500 μm.

I Left panel shows the quantification of EBs size derived from human iPSCs transiently transfected with either control or miR-203 mimics as in panel (H) at different time points during the differentiation process. The percentage of EBs presenting internal large cavities during the indicated time course of differentiation is shown in the right panel. Data are mean ± SEM ($n = 3$ independent experiments). $^{***}P < 0.001$ (Student's *t*-test).

Source data are available online for this figure.

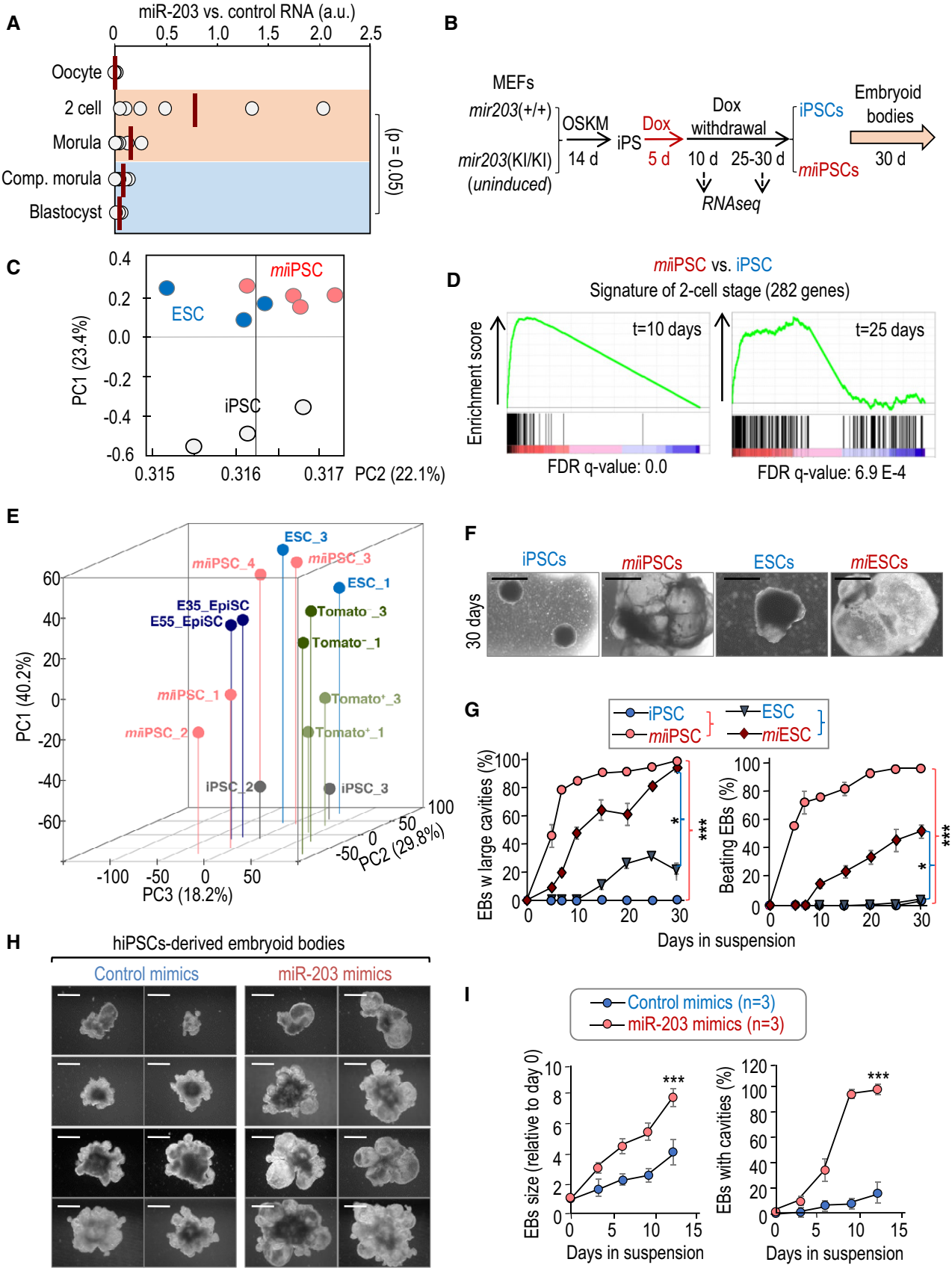

Figure 1.

these iPSC clones as well as wild-type ESCs was analyzed 10 days or 1 month after miR-203 induction (Fig 1B) and surprisingly revealed that *mi*iPSCs were transcriptionally closer to ESCs than Dox-treated wild-type iPSCs both at the genome-wide level (Fig 1C) and when considering a pluripotency-associated signature defined previously (Chung *et al*, 2012) (Fig EV1D). In addition, almost every transcript included in a 282-gene signature of 2C blastomeres (Biase *et al*, 2014) was induced by miR-203 and sustained during 10 days after Dox withdrawal (Figs 1D and EV1E), including genes such as *Zscan4c* previously related to the zygotic transcriptional program (Eckersley-Maslin *et al*, 2019). Importantly, we also assessed the transcriptomes of different clones of *mi*iPSCs, mESCs, 2-cell-like mESC subpopulations (MacFarlan *et al*, 2012; GSE 33923), and epiblast stem cells (Najm *et al*, 2011; GSE 26814) (Fig 1B and E). Principal component analysis revealed a gene expression pattern of *mi*iPSC clones 1 and 2 (analyzed 10 days after miR-203 exposure) similar to that observed for Tomato-positive cells, characterized as 2C-like ESCs by MacFarlan and collaborators, while *mi*iPSC clones 3 and 4 (analyzed 25 days after miR-203 exposure) exhibited a profile more similar to ESC clones, corroborating the observations showed in Fig 1D. An additional comparison of the expression profiles in *mi*iPSCs versus un-induced iPSCs at day 30 after doxycycline withdrawal suggested higher expression of genes related to tissue morphogenesis and embryonic development in those clones in which miR-203 had been transiently induced (Figs 1B and EV1F and Dataset EV1).

The differentiation potential of *mi*iPSCs was directly tested in the embryoid body (EB) formation assay *in vitro*. Transient induction of miR-203 for 5 days followed by 2–4 weeks of Dox withdrawal in either iPSCs (*mi*iPSCs) or ESCs (*mi*ESCs) resulted in a significant increase in EB size accompanied by the formation of large internal cavities (Fig 1F and G, Appendix Fig S1A–C). Furthermore, *mi*iPSC- and *mi*ESC-derived EBs showed beating with higher efficiency and at earlier time points than their untreated counterparts (Fig 1G, Appendix Fig S1C). *mi*iPSC-derived EBs displayed a complex organization with high expression of primitive endoderm (Gata4), mesoderm (Cd34), and ectoderm (Pax6) or neuroectoderm (Nestin) markers (Appendix Fig S1D and E and Movie EV1).

To further validate these observations beyond the genetic model, we tested the effect of transient expression of ectopic miR-203 using a CMV-driven retroviral vector or RNA mimics (Fig EV1G and Appendix Fig S1F and G). These two strategies also resulted in improved EB formation (large cavities, beating) in *mi*iPSCs or *mi*ESCs (Fig EV1G), indicating that these effects were not unique to the inducible genetic model.

Since the combination of the MEK inhibitor PD0325901 and the GSK3 inhibitor CHIR99021 with LIF (2i/L conditions) has been previously shown to render iPSCs closer to ESCs (Ying *et al*, 2008), we also tested the effect of miR-203 under 2i/L conditions. *mi*iPSCs grown in 2i/L also displayed an enrichment in the transcription of stemness factors and developmental pathways when compared to wild-type iPSCs grown in the same conditions (Appendix Fig S2A). In addition, pre-treatment with Dox for 5 days, 2–4 weeks prior to EB assays, of *mi*iPSCs cultured in 2i/L conditions promoted a significant increase in EB size, formation of large internal cavities, and beating (Appendix Fig S2B and C), suggesting an additional effect of miR-203 over the 2i/L conditions.

The expression of miR-203 at the 2-cell stage inspired us to further analyze the early expression of 2C-related endogenous retroviruses in cultured *mi*PSCs. Transient expression of miR-203-GFP in wild-type ES cells significantly increased the number of 2C-like cells as determined by the expression of the murine endogenous retrovirus with leucine tRNA primer (MuERV-L; 2C::Td-Tomato reporter; MacFarlan *et al*, 2012) analyzed 24 h after miR-203 addition (Appendix Fig S3A). In line with these observations, exposure to miR-203 induced the primary expression of genes harboring a proximal upstream or an intronic MERVL element (Appendix Fig S3B).

Of interest, transient exposure to miR-203 mimics also rendered human pluripotent cells to a ground naive state (Appendix Fig S3C and D), as measured by the expression of the family HERVH of human endogenous retroviruses (HERVs) involved in the maintenance of human naive pluripotency (Wang & Gao, 2016). miR-203 mimics induced the expression of the HERVH-GFP reporter in a significant number of colonies, in many cases not only in the periphery but also in almost the totality of the cells of the colony, and such expression was sustained for 5 days in culture. When the differentiation potential of these cultures was tested (several weeks after miR-203 transient expression), human *mi*iPSCs generated significantly bigger EBs with larger internal cavities than the control counterparts (Fig 1H and I), suggesting altogether that the effect of miR-203 can be achieved using delivery systems with independence of the genetic knock-in system and it is also functional in human cells.

miR-203 expands developmental potential and plasticity of PSCs

We then tested the potential of *mi*iPSCs (in which the expression of miR-203 had only been induced for 5 days *in vitro*) to form teratomas either after subcutaneous or intraperitoneal injection. *mi*iPSCs formed significantly bigger tumors in these assays (Fig 2A). Intriguingly, these teratomas were not only bigger but also they contained tissues that are not typically found in control iPSC-induced teratomas, such as bone marrow, pancreas, or cartilage, as well as trophoblast giant cells as confirmed by the expression of PL-1 (Figs 2B and EV2). Transcriptomic studies in these complex structures suggested upregulation of genes involved in embryonic development and organ morphogenesis when derived from *mi*iPSCs (Appendix Fig S4A and Appendix Table S1). Immunohistochemistry studies showed elevated expression of multiple differentiation markers representing ectoderm, mesoderm, and endoderm in *mi*iPSC-derived teratomas (Appendix Fig S4B and C). Interestingly, these teratomas also showed elevated levels of proliferation (as scored by Ki67; Appendix Fig S4D) or pluripotency markers such as Nanog, Oct4, or Sox2 *in vivo* (Appendix Fig S4B), suggesting that these structures contained a complex mixture of undifferentiated cells, expressing stemness markers, together with differentiated cells.

It has been reported that iPSCs generated *in vivo* are able to form small embryo-like structures, containing tissues derived from the three germinal layers in the presence of extraembryonic membranes, when inoculated intraperitoneally (Abad *et al*, 2013). In our hands, wild-type iPSCs generated *in vivo* were able to form embryo-like structures in 11% of injected mice, with an efficiency similar to the one reported previously (Abad *et al*, 2013). However, *mi*iPSCs generated *in vitro* were much more efficient, with 83% of injected mice showing embryo-like structures (Fig 2C). As in the case of *in vivo*-formed iPSCs, *mi*iPSC embryo-like structures were positive for

specific markers of the three embryonic layers (Fig 2D). Brief exposure to miR-203 *in vitro* also improved the formation of chimeras from both *mi*iPSCs and *mi*ESCs, achieving 100% of chimerism efficiency in *mi*ESCs (19 chimeras were obtained out of 19 pups born; Appendix Fig S5). The number of chimeras that reached adulthood and contributed to germline transmission was also notably increased (5–10 times, respectively) in *mi*iPSC- and *mi*ESC-derived mice compared with their respective untreated controls.

The performance of *mi*iPSCs was also tested in the tetraploid complementation assay, one of the most stringent tests for developmental potency. Few iPSCs are efficient in this assay in which any born animal develops uniquely at the expense of exogenous diploid

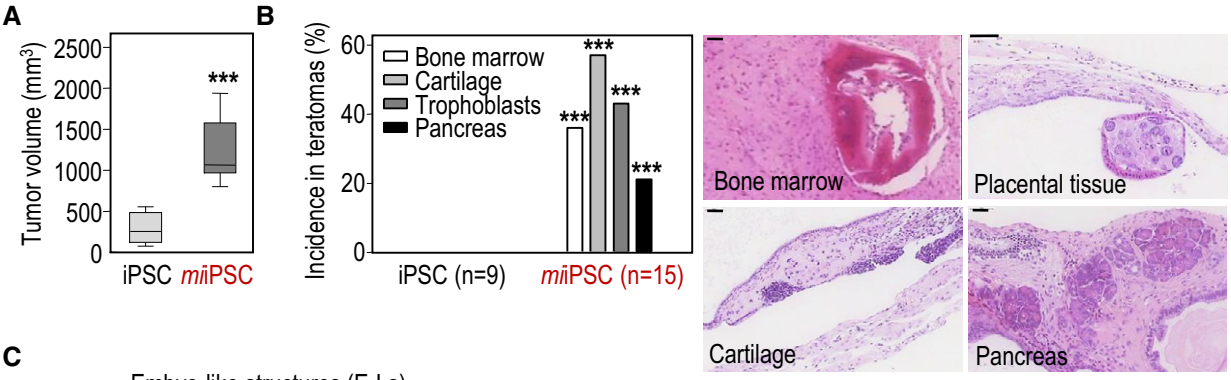

C

Embyo-like structures (E-Ls)

Cells	Nº clones	Mice inoculated	Mice with E-Ls	%
iPSC	8	8	0	0
iv iPSC	9	9	1	11
*mi*iPSC	12	12	10	83

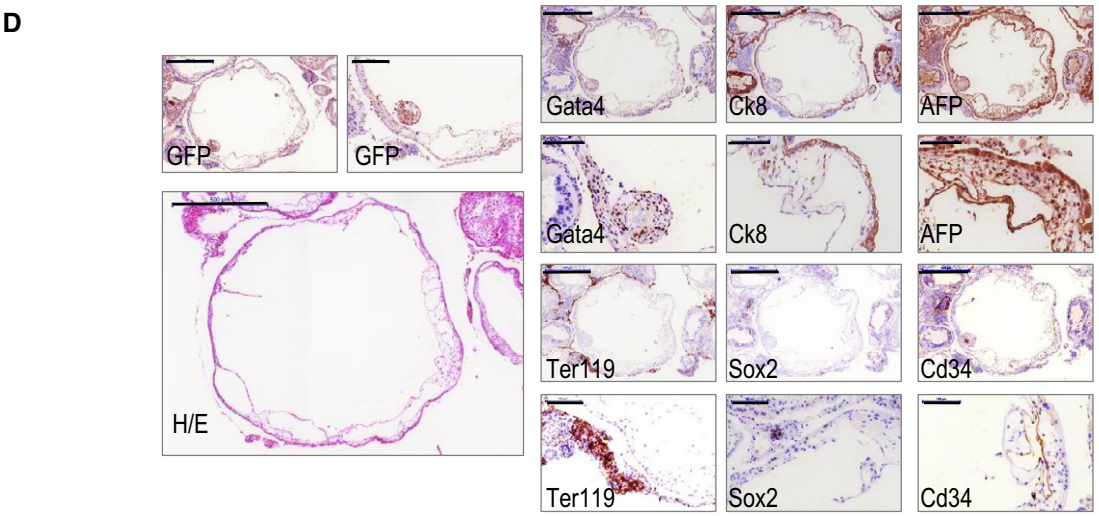

E

Tetraploid complementation assay

Cells	iPSC (n=3)	*mi*iPSC (n=3)	ESC (n=3)
Transferred embryos	69	144	42
Embryos arrested at E10.5-E13.5	10	12	2
Embryos arrested at E15.5-E17.5	1	0	0
"All-iPSC/ESC" mice born	0	4	6
"All-iPSC/ESC" adult mice with G.T.	0	2	5

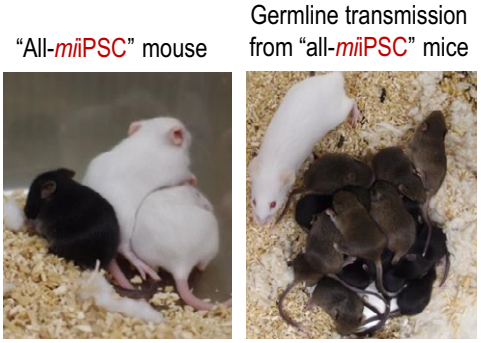

Figure 2.

Figure 2. Transient exposure to miR-203 *in vitro* improves the *in vivo* developmental potential of iPSCs and ESCs.

A Teratoma volume (mm^3) 20–25 days after subcutaneous injection of wild-type iPSCs or *mi*iPSCs expressing GFP. Data are represented as mean ± SEM (n = 8 tumors per genotype; 292.8 ± 66.67 versus 1,216 ± 140.1; difference between means: 923.5 ± 155.2; 95% confidence interval: 1,256 to −590.7); ***$P < 0.001$ (Student's t-test). Representative images are shown in Fig EV2.

B Incidence and representative images of specific highly differentiated tissues in teratomas. The number of tumors included in the analysis is indicated in the panel. ***$P < 0.001$ (Student's t-test). Scale bars, 50 μm.

C Table showing the frequency of nude mice with embryo-like structures (E-Ls) in their abdominal cavity 20–30 days after intraperitoneal (i.p.) injection of 400,000–500,000 *in vivo* (iv)-generated wild-type iPSCs, un-induced iPSCs, or *mi*iPSCs. The number of independent clones tested per condition is indicated in the panel (each animal was inoculated with a different clone).

D Representative example of E-Ls generated after i.p. injection of GFP-expressing *mi*iPSCs. H/E, Hematoxylin and eosin. The following antigens were detected by immunohistochemistry: Sox2 (ectoderm), Cd34 (mesoderm), Gata4 (endoderm), AFP, and CK8 (visceral endoderm of the yolk sac) and Ter119 (nucleated erythroid cells). Scale bars, 500 and 100 μm for higher magnifications.

E Embryo tetraploid complementation assays with un-induced iPSCs, *mi*iPSCs, or wild-type ESCs (n = 3 clones per condition). Pictures on the right show a representative example of a viable "all-*mi*iPSC" mouse (black) generated from *mi*iPSCs and litters obtained from "all-*mi*iPSC" adult mice, which efficiently contributed to germline transmission.

Source data are available online for this figure.

iPSCs (or ESCs) incorporated into a tetraploid embryo. Whereas we did not obtain all-iPSC mice in control iPSCs, the very same clones were able to form all-*mi*iPSC mice after transient *in vitro* exposure to miR-203 (Fig 2E). Importantly, half (2/4) of these "all-*mi*iPSC" mice reached adulthood healthy and were proficient for germline transmission (Fig 2E). Although specific clones of iPSCs have been previously found to contribute to all-iPSC mice (Li *et al*, 2011), it is important to consider that the effect of miR-203 is additive on already-established PSCs providing an easy protocol for enhancing available PSCs.

miR-203 increases human–mouse interspecies chimera competency

The high efficiency of *mi*PSCs in contributing to mouse chimeras led us to test their effect in the formation of interspecies human–mouse conceptuses. Td-Tomato fluorescent-labeled human iPSCs were transiently transfected with pMCSV-miR-203-GFP (human *mi*iPSCs), and cells were maintained at least 1 week in culture to ensure that miR-203 expression was transient and absent before cell injection. To compare the effect of miR-203 in the context of the most efficient protocol reported so far, we cultured these human cells in the presence of human LIF, CHIR99021, (S)-(+)-dimethindene maleate, and minocycline hydrochloride (LCDM), a cocktail recently proposed to enhance the potential of PSCs (Yang *et al*, 2017). We initially injected 15 human iPSCs into 8C-stage mouse embryos and examined its chimeric contribution after 48–60 h of culture *in vitro*. As shown in Appendix Fig S6, pre-exposure of human *mi*iPSCs to miR-203 resulted in 100% of the mouse blastocysts presenting Td-Tomato-positive human cells (also identified with anti-human OCT4 antibodies), whereas this efficiency was only 60% when using control human iPSCs. We next examined the contribution of human iPSCs to interspecies chimeras in similar assays in which injected 8C-stage embryos were allowed to implant (Appendix Fig S7). The presence of human cells in mouse E10.5 conceptuses was identified by immunostaining with anti-human nuclei (HuNu) antibody or by direct detection of fluorescent Td-Tomato. Both HuNu and Td-Tomato-positive areas were significantly increased in embryos injected with *mi*iPSCs when compared to control iPSCs (Appendix Fig S7), suggesting a more efficient contribution of human iPSCs to mouse embryos after brief exposure to miR-203.

To further challenge the system, we injected one single human iPSCs into 8C-stage mouse embryos and examined its chimeric contribution after 48–60 h of culture *in vitro*. As shown in Fig 3A and B pre-exposure of human *mi*iPSCs to miR-203 resulted in 80–100% of the mouse blastocysts presenting Td-Tomato-positive human cells (also identified with anti-human OCT4 and HuNu antibodies), whereas this efficiency was only 54% when using control human iPSCs also cultured in the presence of LCDM but not miR-203. We next examined the contribution of human iPSCs to interspecies chimeras in similar assays in which one human cell-injected 8C-stage embryos were allowed to implant. The presence of human cells in mouse E9.5 conceptuses was identified by immunostaining with anti-human nuclei (HuNu) antibody or by direct detection of fluorescent Td-Tomato, and their proper integration and differentiation into the mouse embryo were corroborated using embryo markers such as Gata4, Sox2, or hSOX17 (Fig EV3C). Both HuNu- and Td-Tomato-positive areas were significantly increased in embryos injected with *mi*iPSCs when compared to control iPSCs (Figs 3C–E and EV3A and B). Altogether, these data suggested a more efficient contribution of human iPSCs to mouse embryos after brief exposure to miR-203.

miR-203 effects are Dnmt3a/b-dependent

To analyze the mechanism by which miR-203 enhances the differentiation capacity of PSCs, we searched for predicted miR-203 targets among the transcripts downregulated in *mi*iPSCs (Fig 4A). As the long-term effects resulting from transient expression of miR-203 suggest an epigenetic mechanism, we selected from the previous list those genes involved in epigenetic regulation of gene expression (GO0040029). We found 18 GO0040029 transcripts downregulated in *mi*iPSCs and predicted as miR-203 targets according to different microRNA target prediction algorithms (Fig 4A and Appendix Table S2). Among these transcripts, the top hits with the highest score as miR-203 targets corresponded to the *de novo* DNA methyltransferases *Dnmt3a* and *Dnmt3b*. These two transcripts were also significantly downregulated after expression of miR-203 mimics in wild-type iPSCs (log2 fold change = −0.24 for *Dnmt3a* and −0.22 for *Dnmt3b* transcripts). Human *miR*-203 and *DNMT3a/b* transcripts have been previously shown to display inverse expression profiles in cancer cells (Sandhu *et al*, 2012; Gasque Schoof *et al*, 2015), and *DNMT3b* was recently shown to be a direct miR-203 target in human colon cancer cells (To *et al*, 2017). Both *Dnmt3a* and *Dnmt3b*

A

	Total embryos	Blastocysts with Td+	Blastocysts with Td+/OCT4+	Percentage of efficiency
Control hiPSCs P31	22	14	12	54.5%
Human *mii*PSCs P29+0	21	17	17	80.9%
Human *mii*PSCs P36+2	30	29	29	96.7%
Human *mii*PSCs P36+4	12	12	12	100%

P=0.02123
P=0.00042
P=0.00042

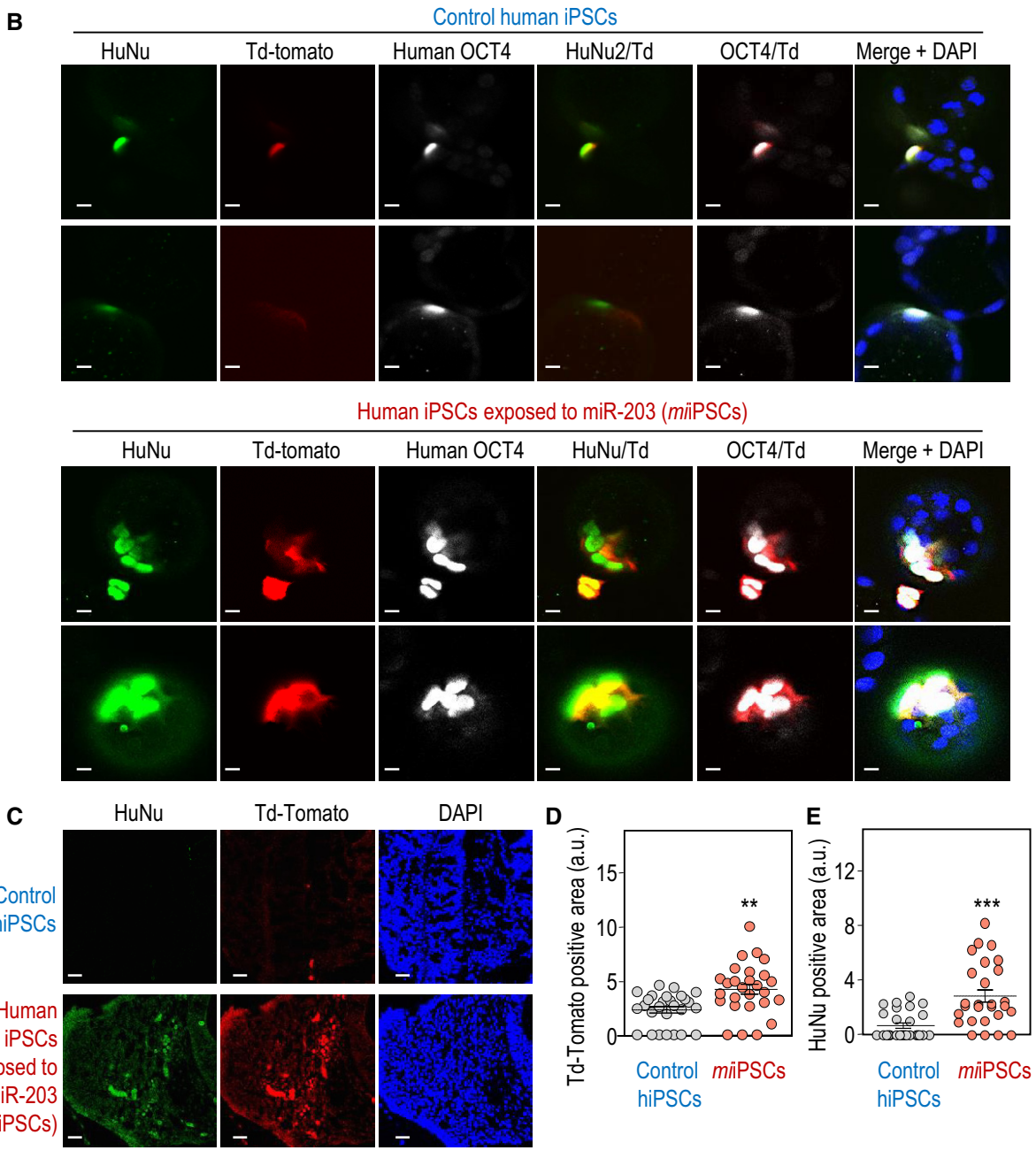

Figure 3.

Figure 3. miR-203-exposed human iPSCs efficiently contribute to human–mouse interspecies chimeras.

A Summary of chimera assays in which one single Td-Tomato fluorescent-labeled human iPSC, either control or transiently transfected with miR-203-expressing vectors (*mi*iPSCs), was injected into 8C-stage mouse embryos and their contribution analyzed 48-60 h later. *P*-values are indicated in the figure (Student's *t*-test).

B Representative images showing the contribution of human control iPSCs or *mi*iPSCs to mouse blastocysts. These structures were co-immunostained with (human) anti-OCT4 and anti-HuNu antibodies. Td-Tomato, red; Scale bars, 50 μm.

C Interspecies chimera assays in which the 8C-stage mouse embryos indicated in (A, B), injected with one single human iPSCs and cultured *in vitro* for 48 h to reach the blastocyst stage, were then transfected to 2.5 days post-coitum pseudo-pregnant females. The post-implantation mouse conceptuses were dissected at the E9.5 developmental stage and analyzed by immunofluorescence. Representative images showing the integration of control human iPSCs (top) or *mi*iPSCs (bottom) into mouse E9.5 embryos. Anti-human HuNu antibody was co-stained with Td-Tomato direct fluorescence to detect human cells in E9.5 mouse embryos. Scale bars, 20 μm.

D, E Quantification of the Td-Tomato-positive (D) or HuNu-positive (E) area in 40-50 different cryosections of these embryos randomly and blindly selected for IF analysis. Data are mean ± SEM $^{**}P < 0.01$; $^{***}P < 0.001$ (Student's *t*-test).

Source data are available online for this figure.

transcripts contain conserved miR-203 sites in their 3′-UTR (Fig EV4A), and exogenous expression of miR-203 led to decreased signal of a luciferase construct fused to these sequences, but not to 3′-UTR sequences from the related genes *Dnmt3l* or *Dnmt1* (Fig 4B and C). The downregulation of these genes was abrogated (Fig 4C) when the putative miR-203-binding sites were mutated (Fig EV4B) indicating a direct control of these transcripts by miR-203. To further confirm the regulation of DNMT3A/B by miR-203, we also tested their protein levels in 5 different clones of mouse un-induced iPSCs or *mi*iPSCs as well as one human cell line, transfected with control or miR-203 mimics, immediately after miR-203 exposure (Fig EV4E).

To test to what extent downregulation of Dnmt3a/b could mimic the effect of miR-203, we knocked down these *de novo* DNA methyltransferases by RNA interference means (*siDnmt3a/b*). RNA sequencing of these samples (following the protocols explained above) revealed that *siDnmt3a*/b iPSCs exhibited a transcriptomic profile closer to *mi*iPSCs (Figs 4D and EV4C). In addition, downregulation of Dnmt3a/b induced the growth, formation of long cavities, and increased beating of EBs to a similar extent to that observed in *mi*iPSC-derived EBs (Fig 4E and F), whereas individual knockdown of these transcripts displayed partial effects (Figs 4E and F, and EV4D). Importantly, the overexpression of miR-203-resistant Dnmt3a and Dnmt3b cDNAs, simultaneously to the transient doxycycline treatment, prevented the overgrowth of *mi*iPSC-derived EBs (Figs 4G and H, and EV4D).

At shorter time points, knockdown of *Dnmt3a/b* also increased the 2C-like population in wild-type ESCs as scored by the expression of the MERVL element (Appendix Fig S8), although to lesser extent than miR-203. Whether these differences are due to variable efficiencies in the control of gene expression of additional miR-203 targets is unclear at present. Moreover, the expression of miR-203-resistant *Dnmt3a/b* cDNAs significantly prevented the expression of the 2C-related marker, as measured 5 days after transfections (Appendix Fig S8). Altogether, these observations demonstrate that Dnmt3a/b *de novo* methyltransferases are miR-203 targets, in both mouse and human PSCs, responsible of at least part of the miR-203-mediated effects.

miR-203 expression results in global and reversible DNA hypomethylation in PSCs

Given the critical role of Dnmt3a/b as *de novo* DNA methyltransferases, we next analyzed the genome-wide methylation profile of

Figure 4. DNA methyltransferases 3a and 3b are miR-203 targets involved in the regulation of PSC potential.

A Venn diagrams representing common genes downregulated in *mi*iPSCs, predicted as miR-203 targets, and also involved in the epigenetic regulation of gene transcription (GO:0040029). The list of the common 18 transcripts (including *Dnmt3a* and *Dnmt3b*) is presented as Appendix Table S2.

B, C Relative luciferase units (RLU; normalized to Renilla luciferase and relative to DNA amount) in 293T cells transfected with DNA constructs carrying the wild-type 3′-UTRs from the indicated transcripts (B) or the mutated versions of *Dnmt3a* and *Dnmt3b* 3′-UTRs, downstream of the luciferase reporter (C). Cells were co-transfected with *Renilla* luciferase as a control of transfection, and a plasmid expressing GFP or miR-203-GFP. Data are represented as mean ± SD ($n = 3$ independent experiments).

D Principal component analysis from RNAseq data including profiles from wild-type iPSCs, *mi*iPSCs, and wild-type iPSCs transfected with either control siRNAs (*siC*), or siRNAs specific against *Dnmt3a* (*siDnmt3a*), *Dnmt3b* (*siDnmt3b*), or both (*siDnmt3a*/b).

E Representative images of embryoid bodies (EBs) derived from wild-type iPSCs in which the expression of *Dnmt3a* and *Dnmt3b* was transiently repressed by siRNAs. Scale bars, 500 μm. Plots show the quantification of the size of EBs and the percentage of EBs with large cavities or beating at different time points during the differentiation process. Data are represented as mean ± SEM ($n = 3$ independent experiments).

F Expression levels of *Dnmt3a* or *Dnmt3b* transcripts after transfection of wild-type iPSCs with specific siRNAs either against *Dnmt3a*, *Dnmt3b*, or a combination of both (*Dnmt3a*/b) (as indicated in E). RNA expression was measured 24 h after the transfection protocols and was normalized by GAPDH mRNA levels. Data are represented as mean ± SEM ($n = 3$ independent experiments).

G Representative images of EBs derived from *mi*iPSCs that were transiently and simultaneously transduced with Dnmt3a and Dnmt3b cDNAs or empty vectors, and simultaneously treated with Dox to induce miR-203 expression. Scale bars, 500 μm. Plots show the quantification of EB size, percentage of EBs with large cavities, and beating EBs at different time points during differentiation. Data are represented as mean ± SEM ($n = 3$ independent experiments).

H Expression levels of *miR-203*, *Dnmt3a*, or *Dnmt3b* transcripts in iPSCs after induction of miR-203 (*mi*iPSCs) and transduced with *Dnmt3a* and *Dnmt3b* cDNAs or empty vectors (as indicated in G). RNA expression was measured 24 h after the transfection protocols and was normalized by a control miRNA (miR-142) or GAPDH mRNA, respectively. Data are represented as mean ± SEM ($n = 3$ independent experiments).

Data information: In (B, C, E–H), $^{*}P < 0.05$; $^{**}P < 0.01$; $^{***}P < 0.001$ (Student's *t*-test).
Source data are available online for this figure.

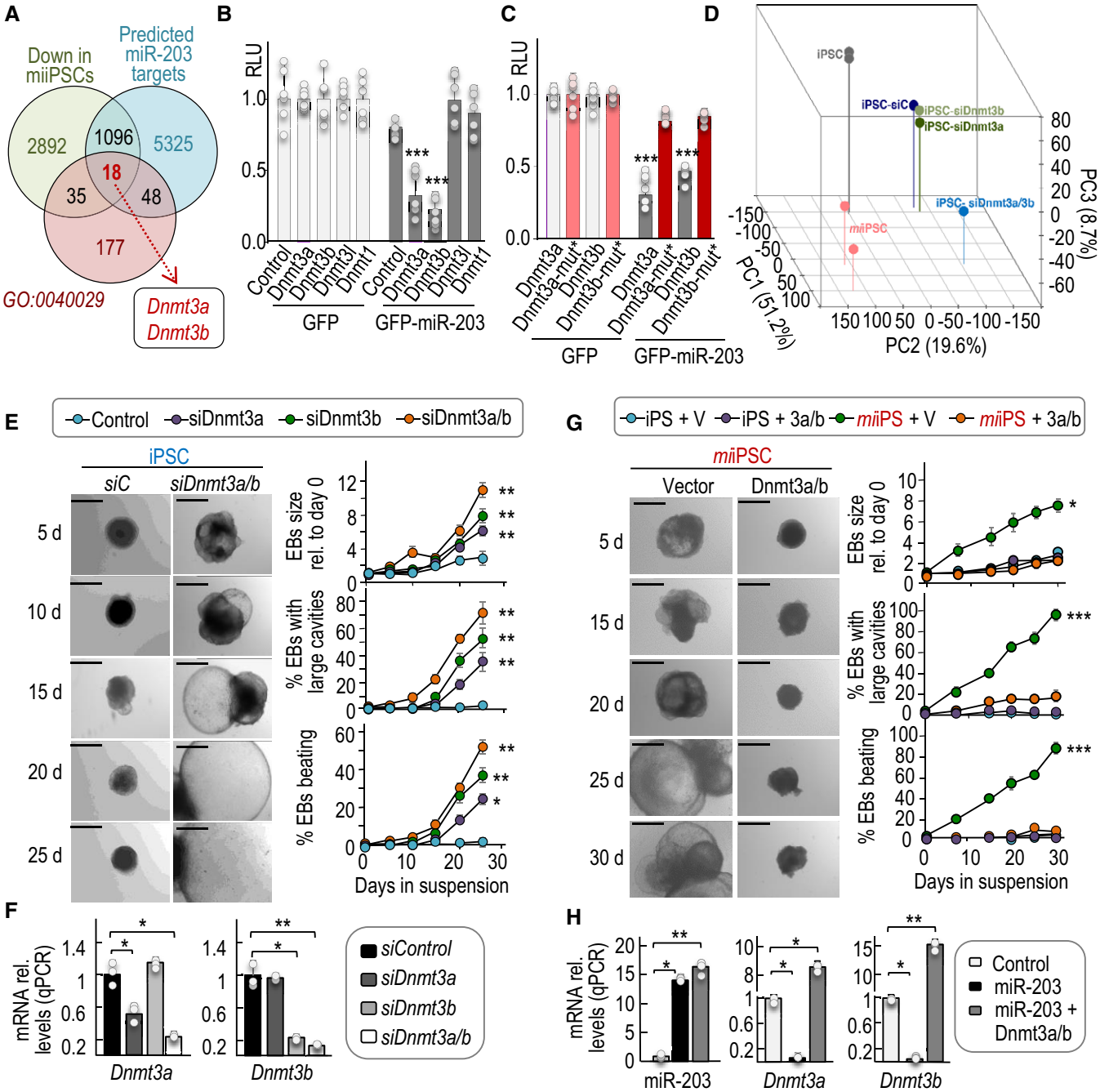

Figure 4.

control (un-induced) iPSCs and *mii*PSCs (after transient induction with Dox) as well as embryoid bodies derived from them (Fig 5A). Wild-type and mutant iPSCs displayed similar levels of methylation before Dox, and wild-type cells were not affected by this treatment. In contrast, transient induction of miR-203 for 5 days resulted in a genome-wide hypomethylation in *mii*PSCs, which was strikingly more prominent 20 days after withdrawal of Dox (t = 25; Fig 5B–E and Datasets EV2 and EV3), a time point in which *Dnmt3a*/b transcript levels had already recovered after their repression in the presence of Dox (Fig EV5A). Notably, the number of DNA methylation valleys (DMVs; (Xie *et al*, 2013) and partially methylated domains (PMDs; (Lister *et al*, 2009) was increasingly higher in *mii*PSCs with time (Fig 5B and Dataset EV3); for instance, 131 PMDs were found at t = 0, while 548 and 6,555 PMD were found at t = 10 and t = 25, respectively. DNA methylation comparison between groups showed that 128 differentially methylated regions (DMRs) out of 131 total DMRs (97.7%; t = 10 versus t = 0) and 12,542 out of 12,549 (99.9%; t = 25 versus t = 0) DMRs were hypomethylated in *mii*PSCs as a consequence of previous exposure to miR-203 (Fig 5E). These gradual changes in methylation spread over a significant proportion of transcription start sites (TSSs) in a genome-wide manner (Fig 5F), and also affected genes of the 2C signature (Fig 5G

and Dataset EV4), in line with the observed upregulation in the expression levels of these 2C markers. Further transcriptional analysis of these samples suggested that deregulated genes with affected DMRs were significantly enriched in chromatin regulators, or genes involved in DNA replication and cell division or embryonic morphogenesis among other pathways (Appendix Fig S9 and Appendix Tables S5 and S6).

As validation of the genome-wide methylation analysis, bisulfite modification followed by clonal sequencing confirmed miR-203-dependent hypomethylation of the promoter region of the gene encoding the E74-like ETS transcription factor 5 gene (*Elf5*), a protein involved in the differentiation of epithelial cells and trophoblast stem cell renewal and differentiation (Latos *et al*, 2015) (Fig EV5B–E). Interestingly, the embryoid bodies derived from *mi*iPSCs displayed higher global levels of DNA methylation and lower number of PMDs (Fig 5B–E) in agreement with the upregulation of *Dnmt3a* and *Dnmt3b* transcripts observed after induction of differentiation (Fig EV5A). In line with the observations at a genome-wide scale, the *Elf5* promoter was hypermethylated in embryoid bodies generated from *mi*iPSCs during the differentiation process (Fig EV5B and C). Previous data suggest that interfering with DNA methyltransferase expression or activity results in global hypomethylation in the genome (Chen *et al*, 2003; Jackson *et al*, 2004; Mikkelsen *et al*, 2008; Blattler *et al*, 2014; Liao *et al*, 2015). Expression of exogenous, miR-203-resistant forms of Dnmt3a/b rescued the hypomethylation observed after miR-203 induction both in the *Elf5* DMRs (Fig EV5D and E) as well as in a DMR located at the histone deacetylase *Sirt6* gene (Fig 5H), suggesting that these *de novo* DNA methyltransferases are critical targets of miR-203 in inducing genome-wide hypomethylation.

Given the recent findings showing that a widespread loss of methylation in PSC cultures might be deleterious when accompanied by massive erasure of genomic imprints (Choi *et al*, 2017a; Yagi *et al*, 2017), we tested the methylation levels at 103 different genes controlled by imprinting control regions (ICRs) in *mi*iPSCs. Whereas *mi*iPSCs displayed a progressive demethylation of genes (red signal at t = 10 and t = 25 in Fig 5I; upper panel), demethylation of ICRs was very limited at t = 10 and moderate at t = 25 in the same samples (lower panel). Importantly, demethylation was in all cases fully recovered upon differentiation (*mi*iPSC-derived EBs; Fig 5I), suggesting that demethylation of *mi*iPSCs, in both DMRs and ICRs, is manageable and reversible, and does not compromise neither the quality of *mi*iPSCs nor their competence to differentiate.

Transient exposure to miR-203 improves differentiation and maturation into cardiomyocytes in a Dnmt3a/b-dependent manner

Since transient expression of miR-203 improves the function of pluripotent cells in several assays, we next decided to directly testing the effect of expressing this miRNA during differentiation of PSCs into cardiomyocytes. The effect of miR-203 was first tested in primary cardiomyocytes isolated from neonatal (P1) rats that undergo further expansion and differentiation when cultured *in vitro*. miR-203 mimics triggered a transient burst of cell proliferation as measured by incorporation of the nucleotide analogue EdU (Fig EV6A) and mitotic markers such as cyclin B1 (Fig EV6B). Importantly, this increase in proliferation occurred in cardiac troponin T (cTnT)-positive cells (Fig EV6C) and resulted in cells with increased ratio of *Myh6* versus *Myh7* myosin heavy chain genes (Fig EV6B), a developmentally regulated switch that correlates with cardiomyocyte maturation and cardiac performance (Miyata *et al*, 2000).

We also tested a cardiomyocyte differentiation protocol from wild-type iPSCs (Kattman *et al*, 2011). Mouse iPSCs were transiently transfected with miR-203 or control mimics, and 15 days later, they were differentiated into cardiomyocytes using specific media and culture conditions (Fig 6A). Transient exposure to miR-203 was accompanied by increased expression of cardiomyocyte differentiation transcripts such as myosin heavy chain (*Myh*), atrial natriuretic peptide (*Nppa*), cardiac troponin T (encoded by the *Tnnt2* gene), and markers for cardiac progenitors such as insulin gene enhancer transcription factors *Isl1* and *Tbx5* in iPSCs previously treated with miR-203 mimics (Figs 6B and EV6D). Importantly, transient exposure to miR-203 resulted in higher expression of not only

Figure 5. Transient expression of miR-203 induces genome-wide hypomethylation in iPSCs.

A Experimental design for the genome-wide DNA methylation analysis of wild-type and *mi*iPSC as well as embryoid bodies (EBs) derived from them. Cells (two independent *mi*iPSC clones and two iPSC technical replicates) were transiently treated with Dox for 5 days and then subjected to Dox withdrawal for 20 additional days before starting the EB formation protocol. Samples for DNA and RNA analysis were collected at the indicated time points before Dox (t = 0), 5 days after Dox withdrawal (t = 10), 20 days after Dox withdrawal (t = 25), or 7 days after starting the EB generation protocol (t = 32 days).

B Genome-wide DNA methylation data showing the number and total size of DNA methylation valleys (DMVs) and partially methylated domains (PMDs).

C DNA methylation distribution of the indicated samples, smoothed over 100-kb blocks.

D Principal component analysis showing the distribution of methylation profiles in the indicated samples (color code as in panel B).

E Number of differentially methylated single CpG sites (DMPs) and differentially methylated regions (DMRs) in the indicated comparisons (color code as in panel B).

F Heat scatterplots representing the mean methylation over all transcripts (transcription start sites, TSSs) in mm10, pairwise for "t = 10 versus t = 0" (left panel) and "t = 25 versus t = 0" (right panel). Note that especially for "t = 25 versus t = 0," most of the points are below the diagonal, indicating broad hypomethylation across most of the genome.

G Heat scatterplots representing the mean methylation over the TSS of the 282 genes included in the 2-cell signature (as in Fig 1D). Analysis as in (F).

H The specific differentially methylated regions (DMRs) at the *Sirt6* locus were analyzed by PCR amplification and sequencing of bisulfite-modified DNA. Ten independent clones were sequenced per condition. The quantification of methylated (filled circles) versus unmethylated (empty circles) CpGs is shown in the histogram in the indicated conditions.

I Heat maps representing the methylation levels at the top differentially methylated regions (DMRs; n = 100; upper panel) or the imprinting control regions (ICRs; n = 103 different imprinting loci; lower panel) in the indicated samples (referred to panels A, B). Color code and scale of DNA methylation, from 0.0 (red) to 1.0 (green), are applicable to both heat maps.

Source data are available online for this figure.

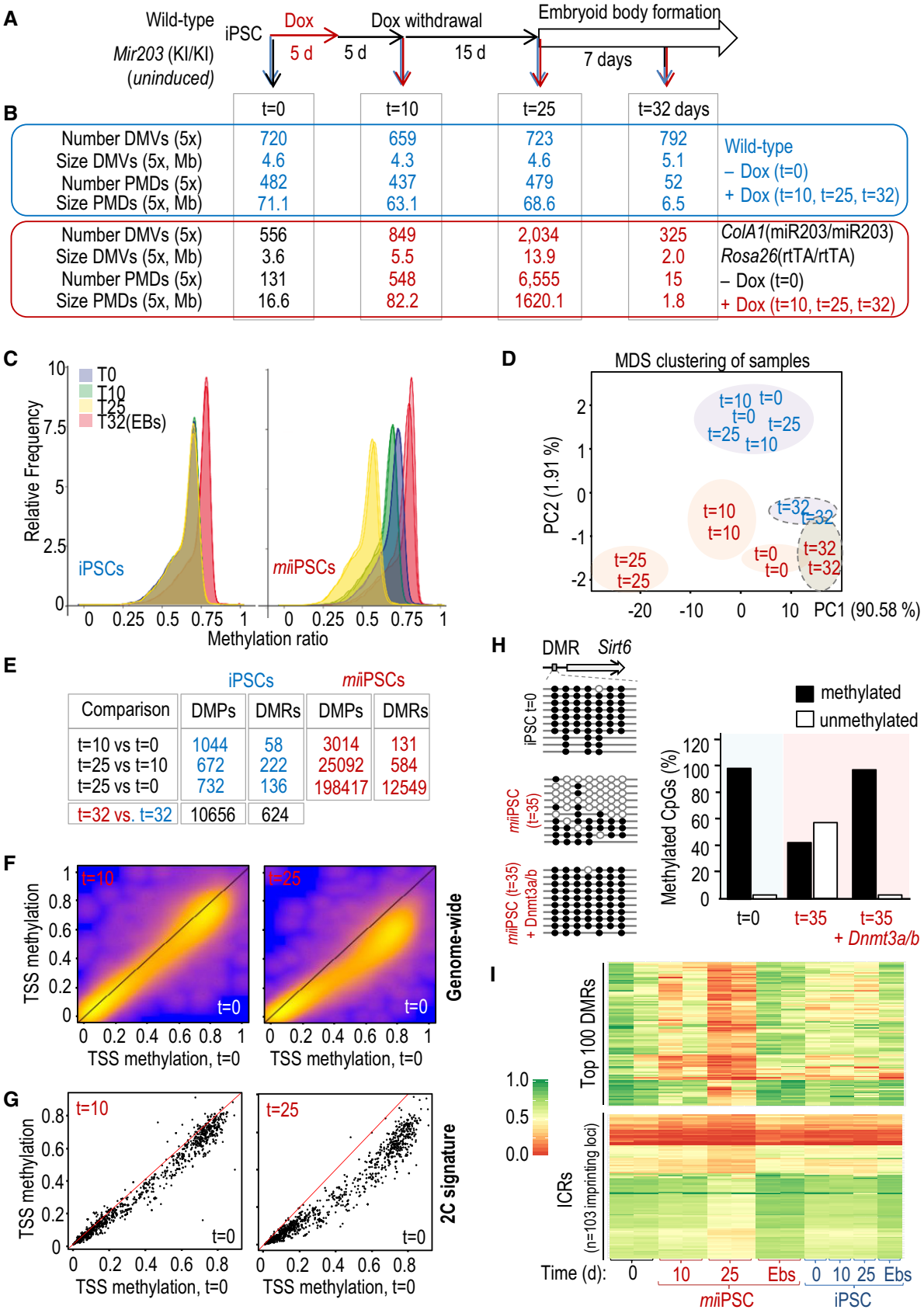

Figure 5.

differentiation but also maturation markers such as the potassium channel components encoded by the *Kcnh2*, *Hcn1*, and *Kcna4* genes (Otsuji *et al*, 2010) that were only minimally induced in cells treated with control mimic RNAs (Fig EV6E). In line with these data, the beating frequency in cardiomyocytes derived from miR-203-treated iPSCs was significantly higher suggesting enhanced functionality (Fig 6C and Movies EV1 and EV2). Expression of miR-203-resistant forms of Dnmt3a and Dnmt3b in parallel to miR-203 (Fig 6A) prevented the upregulation of these differentiation and maturation markers (Fig 6B and D) as well the increase in beating frequency (Fig 6C), suggesting the relevance of the miR-203-Dnmt3a/b axis in functional differentiation and maturation of cardiomyocytes from pluripotent cells.

Discussion

Multiple efforts in the last decade have focused on improving the developmental and differentiation potential of PSCs with the ultimate goal of using these cells in regenerative medicine. PSCs, and in particular iPSCs, are inefficient in the most stringent assays such as tetraploid complementation (Kang *et al*, 2009; Zhao *et al*, 2009) and human–mouse interspecies assays (Mascetti & Pedersen, 2016; Wu *et al*, 2016). Improving culture conditions has been a major subject of research offering multiple options (Choi *et al*, 2017a; Yagi *et al*, 2017; Yang *et al*, 2017). The use of 2i/L clearly improves some properties of PSCs *in vitro* and has been widely used in the last years, although recent data indicate that prolonged use of these

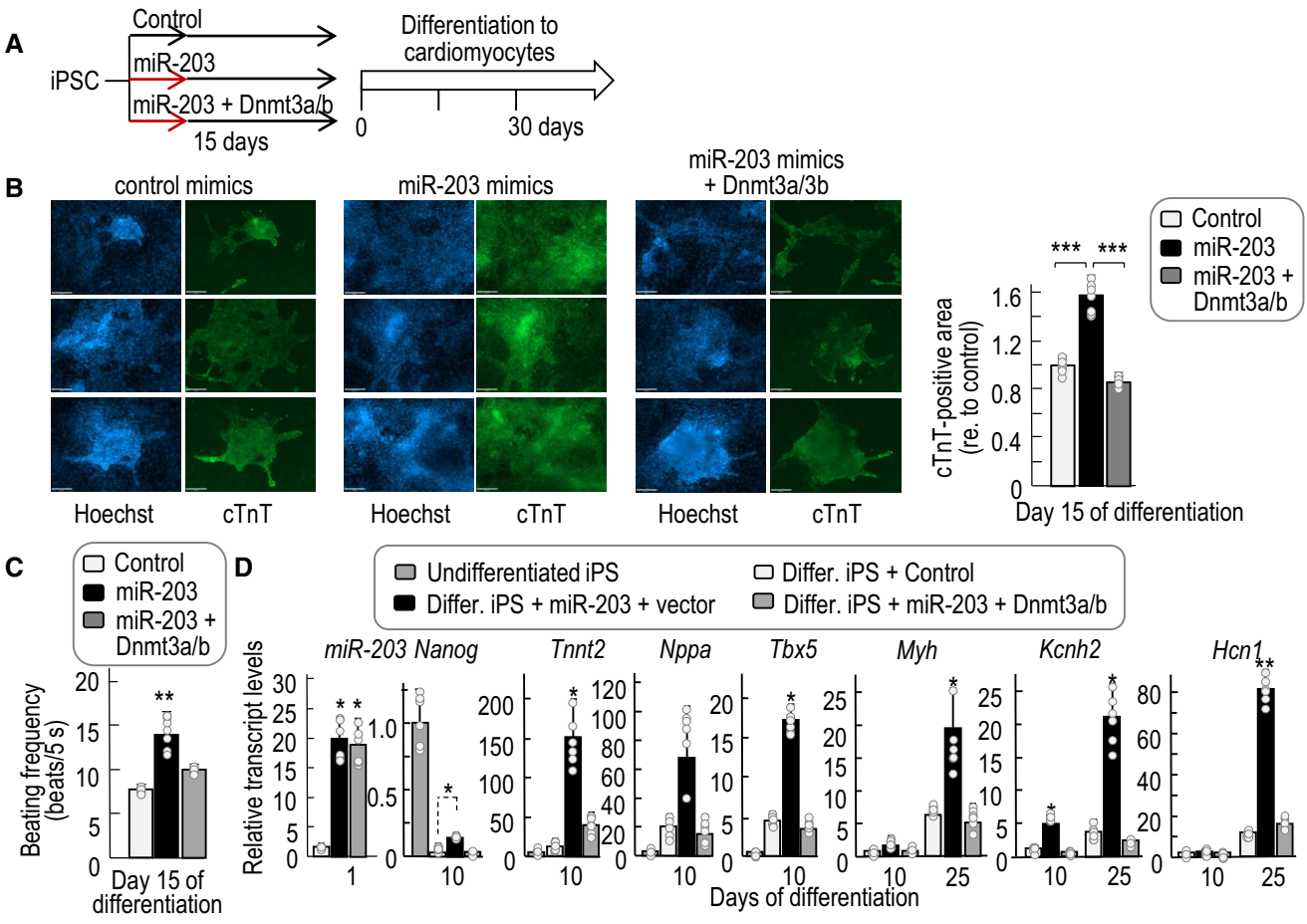

Figure 6. Transient exposure to miR-203 enhances differentiation into mature cardiomyocytes and improves cardiac regeneration.

A Experimental protocol followed for the differentiation of cardiomyocytes from iPSCs in the absence or presence of miR-203 mimics and Dnmt3a/b cDNAs.

B Representative immunofluorescences showing cardiac Troponin T (cTnT, green) and nuclei (Hoechst, blue) staining of *in vitro*-generated cardiomyocytes derived from wild-type iPSCs transiently transfected with either control mimics, miR-203 mimics, or miR-203 mimics + Dnmt3a/b cDNAs. Pictures were taken at day 15 of differentiation. Scale bars, 68 μm. The cTnT-positive area in these cardiomyocytes is shown in the right histogram. Data are represented as mean ± SD (n = 2 independent experiments with 6 replicates each).

C Beating frequency (measured as number of beats per 5 s) of these cardiomyocytes at day 15 of differentiation. Data are represented as mean ± SD (n = 8 independent replicates).

D miRNA or mRNA levels as determined by quantitative PCR of the indicated transcripts at different time points during cardiomyocyte differentiation in the indicated samples. Data are represented as mean ± SD (n = 2 independent experiments with 6 replicates each).

Data information: In (B, C, D), *P < 0.05; **P < 0.01; ***P < 0.001 (Student's t-test).
Source data are available online for this figure.

conditions results in reduced developmental potential *in vivo* (Choi *et al*, 2017a; Yagi *et al*, 2017). Recent alternatives include the use of Src inhibitors or the LCDM cocktail whose targets require further validation (Choi *et al*, 2017a; Yagi *et al*, 2017; Yang *et al*, 2017). Despite these advances, the long-term effects of chemicals that perturb major signaling pathways in the cell remain uncertain. In particular, it will be critical to study how these treatments affect the differentiation potential of PSCs toward specific cell lineages and the functional properties of the resulting cells.

In this work, we report that transient expression of a single microRNA can expand functionality and differentiation plasticity of either mouse or human PSCs both *in vitro* and *in vivo*. Already-established PSCs display enhanced expression of a signature of the top ~280 transcripts characteristic of the 2-cell stage during embryonic development (Biase *et al*, 2014) after brief exposure to miR-203. Importantly, transient exposure to this microRNA results in (i) enhanced differentiation into multiple tissues (e.g., including pancreas, bone marrow, or trophoblast) in teratomas generated *in vivo*; (ii) complex embryo-like structures observed after the injection of these cells into mice; and (iii) augmented efficiency in stringent tests for assessing developmental potency, such as tetraploid complementation assays and human–mouse interspecies chimeras. Remarkably, half of those all-iPSC mice produced with *mi*iPSCs by tetraploid complementation reached the adulthood showing efficient germline transmission, which has been rarely found in previous reports (Okita *et al*, 2007; Kang *et al*, 2009; Zhao *et al*, 2009; Stadtfeld *et al*, 2010a; Leitch *et al*, 2013; Choi *et al*, 2017a; Yagi *et al*, 2017; Yang *et al*, 2017). Similarly, human iPSCs transiently exposed to miR-203 contributed to interspecies human–mouse conceptuses with high efficiency (up to 100% contribution *in vitro*) compared with previous reports (Mascetti & Pedersen, 2016; Theunissen *et al*, 2016; Wu *et al*, 2016). Importantly, miR-203 was able to improve the potential of enhanced pluripotent stem (EPS) cells generated in special culture conditions (Yang *et al*, 2017), suggesting that exposure to this microRNA may be used in combination with other strategies aimed to optimize PSC culture conditions.

Endogenous miR-203 levels are transiently induced during early pre-implantation development, suggesting that this microRNA may contribute to the specific expression profile of early blastomeres. The fact that brief exposure to miR-203 sequences improves the long-term developmental potential of *mi*PSCs even many weeks and passages after its expression suggests an epigenetic mechanism. In fact, *mi*PSCs display a hypomethylated state in chromatin that is self-sustained and accentuated several weeks after exposure to this microRNA implying a replication memory. Among the multiple miR-203 targets, *de novo* DNA methyltransferases Dnmt3a and Dnmt3b likely play an important role in this effect. In cancer cells, miR-203 expression has been previously shown to decrease DNMT3B protein levels leading to *de novo* methylation of cancer-related genes and decrease expression of their products including the xenobiotic transporter ABCG2 (Gasque Schoof *et al*, 2015; To *et al*, 2017). In ESCs, lack of these DNA methyltransferases is known to induce progressive hypomethylation of chromatin with passages (Chen *et al*, 2003; Liao *et al*, 2015) and knockdown of both *Dnmt3a and Dnmt3b* transcripts mimicked the effect of miR-203 in several assays. In addition, the expression of miR-203-resistant Dnmt3a and Dnmt3b cDNAs significantly rescued the phenotypes induced by miR-203 including differentiation to mature cardiomyocytes. Of note, whereas the severe hypomethylation observed in *Dnmt3a*/b knockout cells blocks differentiation (Okano *et al*, 1999; Jackson *et al*, 2004), the hypomethylated state induced by miR-203 is reversible and differentiation is highly improved, when compared to untreated cells, and accompanied of potent *de novo* DNA methylation. Whereas the basis for these differences is unclear, given the promiscuity of microRNAs, miR-203 may have additional targets that could also cooperate with *Dnmt3a*/b repression in the effects of this microRNA in pluripotent cells.

Maintaining methylation of imprinted loci during pre-implantation development is a process mediated by Dnmt1, rather than Dnmt3a or Dnmt3b (Branco *et al*, 2008; Hirasawa *et al*, 2008), in agreement with our data showing a limited effect in the demethylation of ICRs in *mi*PSCs, in which Dnmt1 expression is not modified. Conditions in which ICRs are also demethylated are not appropriate for PSC function as ICR hypomethylation is frequently irreversible (Theunissen *et al*, 2016). In fact, the use of 2i/L conditions results in a widespread loss of DNA methylation including massive erasure of genomic imprints that do not recover methylation after differentiation protocols (Yagi *et al*, 2017) (Yagi *et al*, 2017), leading to defective developmental potential in chimerism studies or tetraploid complementation assays (Choi *et al*, 2017a; Yagi *et al*, 2017). On the contrary, transient exposure to miR-203 induces moderate and reversible ICR hypomethylation that likely contributes to the differentiation and development potential of these PSCs when submitted to differentiation stimuli.

Altogether, our data present miR-203 sequences as an easy-to-use and suitable tool to improve PSCs *in vitro*, by expanding their differentiation and developmental potential *in vivo*. In contrast to other protocols aimed to improve reprogramming into pluripotent cells (Mikkelsen *et al*, 2008; Chen *et al*, 2013; Bar-Nur *et al*, 2014; Li & Izpisua Belmonte, 2016; Takahashi & Yamanaka, 2016), the effects induced by miR-203 can be easily achieved through brief exposure to specific mimics in already-established pluripotent cultures. Together, we conclude that transiently modulating the DNA methylation landscape of *mi*PSCs by short exposure to miR-203 may enhance the performance of these cells in multiple functional assays, including the efficient differentiation and maturation to specific cellular lineages of interest in regenerative medicine.

Materials and Methods

Animal models and procedures

Animal experimentation was performed according to protocols approved by the CNIO-ISCIII Ethics Committee for Research and Animal Welfare (CEIyBA). The miR-203-inducible model was generated by cloning a 482-bp genomic *mmu-mir203* sequence into the pBS31 vector for recombination into the *ColA1* locus in ES cells following the strategy reported previously (Beard *et al*, 2006). The resulting knock-in allele [*ColA1*(miR-203)] was combined with a Rosa26-M2rtTA allele [*Rosa26*(rtTA)] for doxycycline-dependent induction as described previously (Beard *et al*, 2006) (Fig EV1A). These animals were maintained in a mixed C57BL6/J × 129 × CD1 genetic background. For subcutaneous teratomas, iPSCs were trypsinized and 2–3 million cells were suspended in 100 μl PBS

supplemented with 0.1% glucose and were subcutaneously injected into both flanks of athymic nude mice (provided by Charles River). Teratomas were daily controlled and measured by a caliper and finally isolated when their diameters reached 1.5 cm. Animals were euthanized at that point, and teratomas were weighed and processed for RNA extraction or histopathological analysis. For intraperitoneal injections, wild-type athymic mice were injected with 4–5 × 10^5 iPSCs resuspended in 100 μl PBS supplemented with 0.1% glucose. Mice were supervised daily from the day of the injection. Usually, 30 or 40 days after injection mice were euthanized and the visceral teratomas and embryo-like structures were isolated and processed, either for RNA extraction or for histopathological analysis.

For chimera generation, iPSCs or ESCs (5–7 cells per embryo, 10 passages) were microinjected into C57BL/6J-Tyrc-2J/J blastocysts and transferred to Crl:CD1 (ICR) pseudo-pregnant females. For tetraploid complementation studies, 2-cell stage Hsd:ICR(CD-1) embryos were harvested from pregnant females at E1.5 and electrofused in 0.3 M mannitol using a BLS CF-150/B cell fusion instrument with a 250-μm electrode chamber. The electric pulse conditions were 30 V amplitude, 31 μs width, and 1.5 AC voltage. One to two hours later, 1-cell (tetraploid) embryos were selectively picked and cultured in KSOM overnight. Next day, 4-cell stage embryos were selected and aggregated with ESCs or iPSCs. Aggregated embryos were transferred to pseudo-pregnant females 24 h later. To study germline contribution, black ES-iPS mice (from tetraploid complementation assays) were crossed with Albino C57BL/6J-Tyrc-2J/J females and hair coat pigmentation was monitored in the progeny.

Interspecies chimeric assays

Human iPSCs were cultured in serum-free N2B27-LCDM medium under 20% O_2 and 5% CO_2 at 37°C (Yang *et al*, 2017). A total of 500 ml of N2B27 medium was prepared by including 240 ml DMEM/F12 (Thermo Fisher Scientific, 11330-032), 240 ml Neurobasal (Thermo Fisher Scientific, 21103-049), 2.5 ml N2 supplement (Thermo Fisher Scientific, 17502-048), 5 ml B27 supplement (Thermo Fisher Scientific, 12587-010), 1% GlutaMAX (Thermo Fisher Scientific, 35050-061), 1% non-essential amino acids (Thermo Fisher Scientific, 11140-050), 0.1 mM β-mercaptoethanol (Thermo Fisher Scientific, 21985-023), and penicillin–streptomycin (Thermo Fisher Scientific, 15140-122). To prepare the N2B27-LCDM medium, small molecules and cytokines were added in the N2B27 medium as indicated at the following final concentrations: 10 ng/ml recombinant human LIF (L, PeproTech, 300-05), 1 μM CHIR99021 (C, Tocris, 4423), 2 μM (S)-(+)-dimethindene maleate (D, Tocris, 1425), and 2 μM minocycline hydrochloride (M, Santa Cruz Biotechnology, sc-203339). Y-27632 (5 μM; Tocris, 1254) was added 24 h before and after single-cell passage. Human iPSCs were cultured on mitomycin C (Sigma-Aldrich, M4287)-inactivated mouse embryonic fibroblast (MEF) feeder cells (3*10^4 cells/cm^2). The N2B27-LCDM medium was changed every day with fresh LCDM medium. To maintain human iPSCs in an undifferentiated state, we used the following criteria: (i) Avoid plating human cells too sparsely; (ii) use the proper quantity of freshly prepared MEF feeder cells; and (iii) do not allow human cells to overgrow. iPSCs were passaged by Accumax (Innovative Cell Technologies) every 3–5 days (normally at a split ratio ranging from 1:3 to 1:10), and the exact passage day and split ratio should be determined for each cell line specifically.

For transient miR-203 expression, human iPSCs expressing the Tomato reporter were transfected with pMCSV-miR-203-GFP. The cell pellet was resuspended with the nucleofection/plasmid mixture (P3 Primary Cell 4D-Nucleofector Kit, Lonza): 82 μl solution + 18 μl supplement 1 + 2 μg plasmid. The cells were transferred into a cuvette for nucleofection using a 4D-Nucleofector (Program CB150, Lonza) and then seeded on DR4 MEFs. The next day, the cells were gently digested into single cells using Accumax. Suspensions were filtered through a cell strainer (40 μm). Then, the samples were loaded and sorted to harvest GFP^+ and $Tomato^+$ cells on a Becton-Dickinson Fusion sorter. After cell collection, they were plated on DR4 MEFs in N2B27-LCDM medium plus 10 μM Y-27632. The medium was changed the next day without Y-27632.

For interspecies chimeric experiments, human cells were used 1 day before passaging, which showed an optimal undifferentiated morphology and proliferated exponentially. At this time point, the colonies were at sub-confluent density (approximately 70% density of the day the cells should be passaged). 8- to 10-week ICR female mice were superovulated by the treatment of PMSG and 48 h later intraperitoneal administration of hCG. Female mice were then mated with a male for oocyte fertilization. Appearance of plugs was checked in female mice, and 2-cell stage embryos were harvested 1 day after that. 2-cell stage embryos were cultured in KSOM for another 24 h and named E2.5 embryos. At this time, most of the embryos were around 8-cell stage and ready for human EPS cell injection.

Human iPSCs were first rinsed with PBS, then treated with Accumax for 2 min, and subsequently filtered through a cell strainer (40 μm). Cells were then centrifuged at 1,200–1,500 rpm (250–300 *g*) at room temperature for 3 min. The supernatant was removed, and the cells were resuspended in the culture medium at a proper density (2–6*10^5 cells/ml). 10 μM Y-27632 was added into the suspension. The suspension was placed on ice before injection. One individual human cell (or 15 human cells, in Appendix Figs S6 and S7) was microinjected into each E2.5 ICR diploid mouse embryo. Injected embryos were cultured in N2B27-LCDM medium for the first 4 h (in the presence of 10 μM Y-27632), followed by culture for 44–60 h in mixed cell culture medium and KSOM medium at a 1:1 ratio. When the embryo reached the blastocyst stage, approximately 10 injected embryos were transferred to each uterine horn of a 2.5 days post-coitum pseudo-pregnant ICR female, or fixed with 4% paraformaldehyde for immunostaining. Post-implantation embryos were collected at E9.5, rinsed in PBS, followed by embedding, freezing, and slicing (10 μm thick) with a Cryostat.

For immunofluorescence, embryos or slides were fixed in 4% paraformaldehyde (Sigma) at room temperature for 20 min and washed with PBST for 30 min. Samples were then permeabilized with 0.2% Triton X-100 in PBS. After 3 washings, samples were blocked with PBS (Corning, 21-040-CVR) that contained 1% BSA and 0.05% TWEEN-20 at room temperature for 45 min, and then incubated with primary antibodies at 4°C overnight. After 3 washings, secondary antibodies (Jackson ImmunoResearch) were incubated at room temperature for 1 hr. The nuclei were stained with DAPI (Southern Biotech). The following antibodies were used: anti-OCT4 (C30A3) (1:200; Cell Signaling), anti-HuNu (1:200; Novus, NBP2-34342), anti-CDX2 (1:200, CDX2-88; Bio-Genex), anti-Gata4 (1:200; Santa Cruz, C-20), anti-Sox2 (1:200; R&D, AF2108), and anti-hSOX17 (1:200; R&D, AF1924) (Appendix Table S3).

Immunofluorescence images were obtained using a confocal microscope, and signals were then analyzed and quantified using ImageJ.

All the chimeric experiments were reviewed and approved by the Salk Institutional Animal Care and Use Committee (IACUC) and followed the ethical guidelines of the Salk Institute.

Cell culture and gene expression

Primary mouse embryonic fibroblasts (MEFs) were obtained from embryos at E13.5 and cultured in DMEM supplemented with 10% of FBS and penicillin–streptomycin. Cultures were routinely tested for mycoplasma. Regarding the miR-203-inducible model-derived MEFs, reprogramming was promoted on these MEF cultures by non-inducible Oct4-Sox2-Klf4-cMyc (OSKM) lentiviral transduction. For lentiviral transduction, we transfected HEK293T cells with FUW-OSKM (Addgene #20328) and packaging vectors using Lipofectamine 2000 (Invitrogen). Viral supernatants were collected twice a day on two consecutive days starting 24 h after transfection and were used to infect MEFs, previously plated at a density of 250,000 cells per well in 6-well plates. Previous to infection, polybrene was added to the viral supernatants at a concentration of 2 μg/ml. For all those experiments in which miR-203 was expressed in WT iPSCs by mimic transfection or retrovirus transduction, WT MEF reprogramming to obtain WT iPSCs was performed using inducible OSKM lentiviral transduction (TetO-FUW-OSKM; Addgene #20321). Infected MEFs were then cultured in iPSC medium, containing KO-DMEM (Gibco), 2-mercaptoethanol 50 mM (Invitrogen), non-essential amino acid MEM NEAA (Invitrogen), penicillin and streptomycin (5,000 μg/ml, Invitrogen), Lif (leukemia inhibitor factor, ESGRO, Millipore), and 20% knockout serum replacement (KSR, Invitrogen). In this case, doxycycline was also added to the iPSC medium to promote reprogramming only for the generation of WT iPSCs to be treated with miR-203 mimics or retroviruses (but never in the case of iPSCs derived from the miR-203-inducible animal model, in which miR-203 expression depends on DOX addition). Medium was changed every 24 h, and plates were stained for alkaline phosphatase activity to assure the efficiency of reprogramming (AP Detection Kit, Sigma-Aldrich). Once colonies were picked, iPSCs were cultured in iPSC media over mitomycin C (Roche)-inactivated feeder cells. G4 ESCs were cultured over mitomycin C-inactivated feeders and in the presence of ESC medium containing KO-DMEM, 2-mercaptoethanol, non-essential amino acids, GlutaMAX, penicillin and streptomycin, Lif, and 10% fetal calf serum (HyClone). When indicated, the culture media for pluripotent cells included 2i factors (MEK inhibitor PD0325901 1 μM, Gsk3 inhibitor CHIR99021 3 μM) and mouse LIF (as above) in N2B27 medium, as described previously (Ying *et al*, 2008). For inducing transient miR-203 overexpression, *ColA1*(miR-203/miR-203); *Rosa26*(rtTA/rtTA) iPSC or ESC cultures were treated with Dox (1 μg/ml; Invitrogen) during 5 days. After that, Dox withdrawal was standardized for the cultures during following several passages (10–30 days) unless other time points are indicated in the text. In this inducible system, we always test that insert expression is uniquely dependent on Dox, and becomes absolutely undetectable after Dox withdrawal. As a control of the treatment itself, Dox was also added and tested in wild-type iPSCs or ESCs.

For overexpression experiments, miR-203 and full-length cDNAs of Dnmt3a and Dnmt3b were subcloned into the retroviral vector pMCSV-PIG (Abad *et al*, 2013) by restriction-directed subcloning, using pCMV-Sport6-mDnmt3a (MGC clone: 5662) and attB-mCh-mDnmt3b-Poly (A)-NeoR (Addgene plasmid 65553) as templates, respectively. For retroviral transduction, we transfected HEK293T cells with the respective pMCSV-PIG vector expressing a GFP reporter (including either only GFP; miR-203-GFP; Dnmt3a-GFP or Dnmt3b-GFP) and the packaging vector pCL-ECO, using Lipofectamine 2000 (Invitrogen). Viral supernatants were collected twice a day on two consecutive days starting 24 h after transfection and were used to infect either ESCs or IPSCs, previously plated over feeders in 6-well plates. Preceding the infection, polybrene was added to the viral supernatants at a concentration of 2 μg/ml. When transduced with these retroviral vectors, both ESCs and iPSCs were sorted by FACS and GFP-positive cells were selected for subsequent cultures and analysis. For transfection with mimics, we used miRIDIAN microRNA human hsa-miR-203a-5p (C-302893-00)/has-miR-203a-3p (C-300562-03) mimics or mimic transfection control (scramble sequences purchased from GE Dharmacon) with Dy547 (CP-004500-01), all of them from GE Dharmacon. Transfection was performed using either DharmaFECT transfection reagent (Dharmacon) or Lipofectamine RNAiMAX (Invitrogen) following the manufacturer's instructions. Transfection efficiency was evaluated 24 h post-transfection by Dy547 fluorescence, and experiments were then performed as indicated in the figures.

Regarding the use of the two mature forms of miR-203 mimics: As happens with many other microRNAs, two mature microRNAs can originate from opposite arms of the same pre-miRNA, has-miR-203a, which are denoted with a -3p or -5p suffix. However, the mature microRNA found from one arm of the hairpin is usually much more abundant than that found from the other arm, in which case, an asterisk following the name indicates the mature species found at low levels from the opposite arm of a hairpin. In the case of miR-203, the most abundant mature form is miR-203a-3p, while the low abundant form is called miR-203a-5p*.

Human miR-203 is expressed from chromosome 19. Its murine counterpart, mmu-miR-203 (Accession in miRbase MI0000246), is expressed from chromosome 14 of Mus musculus. The main mature sequence of mmu-miR-203, mmu-miR-203-3p (Accession in miRbase MIMAT0000236), seems to be identical to that of hsa-miR-203a-3p. There are experimental evidences of a second mature sequence, mmu-miR-203-5p* (Accession in miRbase MIMAT0004547), which is shorter than hsa-miR-203a-5p (22 nucleotides instead of 25) and differs slightly from its human counterpart in the rest of the sequence (in position 11, G is replaced by A in hsa-miR-203a-5p*). Both miR-203a-3p/-5p were used in these assays, aiming to faithfully mimic the endogenous scenario in which both mature forms are expressed. However, the most abundant form (miR-203a-3p) is responsible for the observed effects, as depicted for example in the Appendix Fig S10.

For RNA interference assays, ON TARGETplus SMARTpool for non-targeting control siRNA (D-001810-01, 02, 03, 04), *Dnmt3a* siRNAs (J-065433-09, 10, 11, 12), and *Dnmt3b* siRNAs (J-044164-05, 06, 07, 08) from Dharmacon were used. Transfection was performed using DharmaFECT transfection reagent (Dharmacon) following the manufacturer's instructions. Transfection efficiency was evaluated 24 h post-transfection by qPCR, using the primers indicated in Appendix Table S4. A few weeks after transfection, the cells were assessed for differentiation to embryoid bodies.

Luciferase-reported assays were performed in HEK293T cells. Briefly, 200.000 cells per well were seeded on 6-well plates, and the

day after, cells were transfected using Lipofectamine 2000 (Invitrogen), following the manufacturer's instructions. The 3′-UTR regions from the murine genes *Dnmt3a, Dnmt3b, Dnmt3l,* and *Dnmt1* were amplified by PCR with specific primers (Dnmt3a_EcoRI-Fw: 5′-GAATTCAGGGACATGGGGGCAAACTGAA-3′ (SEQ ID NO: 55); Dnmt3a_NdeI-Rv: 5′-CATATGCTGAGGCAGTCATTTTAGATTCAT-3′ (SEQ ID NO: 56); Dnmt3b_EcoRI-Fw: 5′-GAATTCTTTTAGCTCACCT GTGTGGGG-3′ (SEQ ID NO: 57); Dnmt3b_NdeI-Rv: 5′-CATATGCCA GAAAGGTAAACTCTGGGCA-3′ (SEQ ID NO: 58); Dnmt3l_EcoRI-Fw: 5′-GAATTCGAAATGAATCACCATAAGATGAAAG-3′ (SEQ ID NO: 59); Dnmt3l_NdeI-Rv: 5′-CATATGAACAATCCTATGATATATTTGAA AAA-3′ (SEQ ID NO: 60); Dnmt1_EcoRI-Fw: 5′-GAATTCGTGCTCT CACCCAGAGCCCCA-3′ (SEQ ID NO: 61); and Dnmt1_NdeI-Rv: 5′-CATATGGCTTGACAGAAGCGCTTTATTTTG-3′) (SEQ ID NO: 62) (Appendix Table S4), using cDNA clones (pCMV-Sport6-mDnmt3a, cDNA clone MGC:5662; pBluescript-mDnmt3l, RIKEN clone: 2410006021; pYX-Asc-mDnmt1, MGC clone: 62302) or mouse cDNA (in the case of *Dnmt3b*). PCR products were verified by sequencing and ligated into the pGL3-Control vector (Promega), downstream of the luciferase reporter gene. Mutations in the miR-203-binding sites were generated by site-directed mutagenesis and subsequently verified by sequencing. Transfections were performed with either pMCSV-GFP or pMCSV-miR-203-GFP vectors, in combination with the pGL3-derived vectors, and Renilla as a control. Luciferase measurement was achieved 48 h post-transfection using a luminescence microplate reader (Bio-Tek).

Murine ESCs expressing the *2C::*Td-Tomato reporter to detect endogenous expression of the 2C-stage retrotransposon MuERV-L were cultured in 2i media over feeders as reported previously (MacFarlan *et al*, 2012). Human iPSCs expressing the long terminal repeat (LTR7) of HERVH endogenous retroviruses fused with GFP reporter (Wang & Gao, 2016) were cultured in mTeSRTM1 media (Stem Cell Technologies) over a Matrigel basement (Corning). Experimentation with human cells was performed according to protocols approved by the ISCIII Ethics Committee for Research (CEI; number PI 61_2017) and the Salk Institute Ethics Committee for Research.

Embryoid body generation

Briefly, iPSCs or ESCs were trypsinized and resuspended to a concentration of 200,000 cells/ml in the presence of complete growth medium lacking leukemia inhibitory factor (Lif). Small drops of this suspension (~35 μl) were collected and seeded on the lid of a 10-mm plate, generating hanging drops of approximately 5,000 cells per drop. After 4 days, the aggregates were already visible at the bottom of the drops and were picked and transferred to a non-adherent plate, containing DMEM and 10% fetal calf serum. There they were maintained in suspension for the indicated times, and beating, size, and cavity formation were assessed every 5 days as described in the figures. Between 20 and 30 EBs were analyzed per condition, and the percentage of beating EBs or EBs with large cavities was calculated for every time point. EB size was measured using the Image J software.

Immunofluorescence and immunohistochemistry

Cells previously seeded in cover slips were fixed in 4% paraformaldehyde for 15 min, permeabilized using PBS 0.1% Triton X-100 for 15 min, and blocked in BSA for 1 h at room temperature. Primary antibody incubation was performed overnight at 4°C in all cases, followed by secondary antibody incubation for 1 h at room temperature. Nuclear staining was included in the last PBS wash, using Hoechst or DAPI. Primary antibodies used in this study were against Cd34 (Abcam), Gata4 (Santa Cruz), Pax6 (Abcam), Nestin (Millipore), cTnT (Abcam), and phospho-histone H3 (Millipore) (Appendix Table S3). Cells were examined under a Leica SP5 microscope equipped with white light laser and hybrid detection.

For immunohistochemistry, tissue samples were fixed in 10% neutral buffered formalin (4% formaldehyde in solution), paraffin-embedded and cut at 3 μm, mounted in SuperFrost® Plus slides, and dried overnight. Consecutive sections were stained with hematoxylin and eosin (H&E) or subjected to immunohistochemistry using automated immunostaining platforms (Ventana Discovery XT, Roche, or Autostainer Plus Link 48). Antigen retrieval was first performed with high or low pH buffer depending on the primary antibody (CC1m, Roche, or low pH antigen retrieval buffer, Dako), endogenous peroxidase was blocked (peroxide hydrogen at 3%), and slides were incubated with primary antibodies against Nanog (Cell Signaling Biotechnology, 8822) cytokeratin 8 (CK8; CNIO Monoclonal Antibodies Core Unit, AM-TROMA I), GFP (Roche, 11814460001), Sox2 (Cell Signaling Technology, 3728), alpha-fetoprotein (AFP; R&D Systems, AF5369), Oct4 (Santa Cruz Biotechnology, sc-9081), KI-67 (Master Diagnostica, 0003110QD), Nestin (Millipore, MAB353), Cd31 (Abcam), Cd34 (ABCAM ab8158), Cd73 (Cell Signaling Technology), collagenase type I (Rockland), Gata4 (Santa Cruz Biotechnology, sc-1237), smooth muscle actin (Thermo Scientific, RB-9010-PO), skeletal actin (Dako, M0635), or Ter119 (LY-76; BD Bioscience, 550565) (Appendix Table S3). Secondary antibodies were conjugated with horseradish peroxidase (OmniRabbit, Ventana, Roche), the immunohistochemical reaction was developed using 3,30-diaminobenzidine tetrahydrochloride (DAB) as a chromogen (chromoMap DAB, Ventana, Roche, or DAB solution, Dako), and nuclei were counterstained with Carazzi's hematoxylin. Finally, the slides were dehydrated, cleared, and mounted with a permanent mounting medium for microscopic evaluation. The images were acquired with a slide scanner (Axio Scan Z1, Zeiss). Images were captured and quantified using the Zen Software (Zeiss).

Western Blot

For Western blotting, cells were lysed in RIPA or a buffer containing 50 mM Tris–HCl, pH 7.5, 1 mM phenylmethylsulphonyl fluoride, 50 mM NaF, 5 mM sodium pyrophosphate, 1 mM sodium orthovanadate, 0.1% Triton X-100, 1 μg/ml leupeptin, 1 mM EDTA, 1 mM EGTA, and 10 mM sodium glycerophosphate. Thirty micrograms of total protein was separated by SDS–PAGE and probed with primary antibodies against Dnmt3a (Novus Biological, 64B1446), Dnmt3b (Novus Biological, 52A1018), or vinculin (Sigma, V9131).

Analysis of mRNA and microRNA levels

RNA was extracted from cell or tissue samples with TRIzol (Invitrogen) or by using the mirVana miRNA Isolation Kit (Thermo Fisher), following the manufacturer's recommendations. Retrotranscription into cDNA was performed using M-MLV Reverse Transcriptase (Promega) following the manufacturer's protocol. Quantitative

real-time PCR was performed using SYBR Green Power PCR Master Mix (Applied Biosystems) in an ABI PRISM 7700 Thermocycler (Applied Biosystems). The housekeeping gene *Gapdh* was used for normalization. The oligonucleotide primers used in this manuscript are listed in the Appendix Table S4. For reverse transcription of microRNAs, we used the TaqMan small RNA assay (4366596), including the specific oligonucleotides for mmu-miR-203-5p and 3p (002580 and 000507), miR-16, and the housekeeping RNA sno-202 or sno-142. Conditions for miRNA amplification were as follows: 30 min at 16°C; 30 min at 42°C; and a final step of 5 min at 85°C. Quantitative real-time PCR was then performed using the TaqMan Universal PCR Master Mix (434437) following the manufacturer's instructions in an ABI PRISM 7700 Thermocycler (Applied Biosystems).

For RNAseq, total RNA was extracted using the miRVana miRNA Isolation Kit (Thermo Fisher), following the manufacturer's recommendations. Between 0.8 and 1 μg of total RNA was extracted from iPSCs, ESCs, or teratomas, with RIN (RNA integrity number) numbers in the range of 9 to 10 (Agilent 2100 Bioanalyzer). Poly A+ fractions were purified and randomly fragmented, converted to double-stranded Cdna, and processed using the Illumina's "TruSeq Stranded mRNA Sample Preparation Part # 15031047 Rev. D" Kit. The adapter-ligated library was completed by PCR with Illumina PE primers (8–11 cycles), and the resulting directional cDNA libraries were sequenced for 50 bases in a single-read format (Illumina HiSeq 2000) and analyzed with Nextpresso (Graña *et al*, 2017). Reads were quality-checked with FastQC (http://www.bioinformatics.babraham.ac.uk/projects/fastqc) and aligned to the mouse genome (GRCm38/mm10) with TopHat-2.0.10 (Trapnell *et al*, 2012), using Bowtie 1.0.0 (Langmead *et al*, 2009) and SAMtools 0.1.19 (Li & Durbin, 2009), allowing two mismatches and five multihits. Transcripts assembly, estimation of their abundances, and differential expression were calculated with Cufflinks 2.2.1 (Trapnell *et al*, 2012), using the mouse genome annotation dataset GRCm38/mm10 from the UCSC Genome Browser (Rosenbloom *et al*, 2015). A false discovery rate (FDR) of 0.05 is used as threshold for significance in differential expression. Heat maps were later built using GENE-E (http://www.broadinstitute.org/cancer/software/GENE-E/index.html). Published datasets (MacFarlan *et al* (GSE 33923); Najm *et al* (GSE 26814) (Yang *et al*, 2017)) were compared using the "Feature Specific Quantile Normalization" method that allows to perform a cross-platform normalization (Franks *et al*, 2018).

Bisulfite conversion, genome-wide DNA methylation, and validation of DMRs

DNA samples were prepared for whole-genome bisulfite sequencing using the TrueMethyl® Whole Genome Kit (CEGX®) according to the manufacturer's instructions. Briefly, 200 ng of genomic DNA was sheared to 800 bp using M220 Focused-ultrasonicator™ (Covaris®). Then, the fragmented DNA was denatured and oxidized by a chemical oxidant to convert 5-hydroxymethyl cytosine to 5-formylcytosine (5fC). The purpose of the oxidation was to ensure that we purely captured the information for 5′ methyl cytosine methylation and not an indistinguishable pattern combination of 5′methyl cytosine and 5′hydroxymethyl cytosine. Following oxidation, the DNA was subjected to bisulfite conversion for the deamination of cytosines and 5fC to uracils. Bisulfite-converted DNA was desulfonated and purified to then proceed to library preparation. In this "post-bisulfite conversion" library preparation method, the fragmented single-stranded bisulfite-converted DNA was adapted with sequencing adaptors at the 3′end followed by an extension step and finally ligation of adaptors at the 5′ end of the molecules. Finally, the libraries were indexed and amplified. The PCR was performed for 10 cycles followed by bead-based purification. An additional purification and size selection step using Agencourt AMPure XP beads (Beckman Coulter, Cat: A63881) were performed to remove adaptor dimers. The purified library was eluted in a final volume of 14 μl pure water. Quality of the library obtained was checked using the DNA High Sensitivity Chip on the Agilent Bioanalyzer. The library was quantified using Qubit and KAPA Biosystems Library Quantification Kit (#KK4824) according to manufacturer's instructions. A total of 1-2pMol of multiplexed libraries were sequenced on a 125-bp paired-end format (Illumina HiSeq 2500). Adapter sequences were removed using Cutadapt version 1.9.1 (Martin, 2011) in paired-end mode with parameters "-m 15 -u 6 -U 6". Bwameth (preprint: Pedersen *et al*, 2014) was then used to align reads to mm10 using default parameters. PCR duplicates were removed using Picard v1.91 (http://broadinstitute.github.io/picard). Count tables of the number of methylated and unmethylated bases sequenced at each CpG site in the genome were constructed using the "tabulate" module of bwa-meth and BisSNP-0.82.2 (Liu *et al*, 2012) with default parameters. All libraries passed basic quality control checks with a minimum of 82.7% of read pairs aligning uniquely. DMRs were called using the WGBS module of DMRcate (Peters *et al*, 2015) with parameters lambda = 1000 and C = 50; DMPs were called using DSS (Feng *et al*, 2014); PMDs, LMRs, and UMRs were called using MethylSeekR (Burger *et al*, 2013); and PMDs were called using the R package "aaRon" (https://github.com/astatham/aaRon).

For the validation of DMRs, clonal bisulfite sequencing was performed at two particular loci: *Elf5* (chr2: 103, 423, 778-103, 424, 180) and *Sirt6* (chr10: 81, 624, 595-81, 625, 547) promoter regions. 100 ng of DNA was bisulfite treated using EZ DNA Methylation-Lightning™ Kit (Zymo Research) following manufacturer's instructions. Triplicate PCR amplifications were then performed using semi-nested bisulfite conversion-specific primers listed in Appendix Table S4, following the PCR conditions previously described for *Elf5* (Lee *et al*, 2011) or using the following protocol: 95°C 4 min; 5 cycles (95°C 45 s, 54°C 1.5 min, 72°C 2 min); 25 cycles (95°C 45 s, 54°C 1.5 min; 72°C 1.5 min); and final extension at 72°C 4 min, for *Sirt6*. The methylation status of the PCR amplicons was determined by the Sanger clonal sequencing of the pooled PCR products to ensure representative clonal analysis using between 8 and 10 clones per sample. The analysis of the methylation status of the clones was performed using BiQ Analyzer (Bock *et al*, 2005).

Neonatal cardiomyocyte isolation and differentiation studies

Neonatal mouse and rat cardiomyocytes were prepared as described previously (Huang *et al*, 2015). Briefly, neonatal cardiomyocytes were isolated by enzymatic disassociation of 1-day-old neonatal mouse or rat hearts with the Neonatal Cardiomyocyte Isolation System (Cellutron Life Technology). Cardiomyocytes were preplated for 2 h to remove fibroblasts. Cells were then plated on 1% gelatin-coated plates in medium containing 10% horse serum and 5% fetal calf serum. Eighteen hours after plating, cells were changed

into serum-free medium and then transfected with 50 nM miR-203a-3p and 5p mimics or control mimics (from Dharmacon) by using Lipofectamine RNAiMAX transfection reagent, following the manufacturer's instructions. Six hours later, media with transfection reagent were removed and substituted by media containing 1% serum. Different time points (as indicated) were collected for subsequent RNA extraction and EdU staining/immunofluorescence. For EdU staining, we used the Click-iT EdU Staining Kit (Invitrogen) following the manufacturer's recommendations. After that, immunofluorescence of cardiomyocyte markers (Troponin T) was performed and Hoechst was finally used for nuclei staining.

For *in vitro* differentiation from mouse iPSCs to cardiomyocytes, wild-type mouse iPSCs were transfected with either control or miR-203 mimics prior to differentiation. In some experiments, additionally pMCSV-Dnmt3a and 3b or empty pMCSV vector was transiently transduced, 24 h after mimic transfection. iPSCs were then maintained in culture under 2i/Lif media for 15 days, before differentiation started. Then, cells were plated in Matrigel pre-coated 6-well plates. Once they become confluent, the media were changed to RPMI 1640/B27 medium (Thermo Fisher Scientific, 61870127 for the RPMI 1640 media and A1895601 for B27) with CHIR99021 5 μM (Stem Cell Technologies, 72054). After 2 days, cells were washed and media without CHIR99021 were added. At day 3 of differentiation, media were supplemented with IWR1 5 μM (Stem Cell Technologies, 72564) and maintained in these conditions for 2 more days. At day 7 of differentiation, the media were changed to RPMI 1640/B27 plus insulin. Then, from day 9 to day 15, cells were cultured in RPMI 1640/B27 and the media were changed every 2 days. From day 16 to day 18 of differentiation, cells were cultured in DMEM without glucose and with lactate 4 mM. From day 18 to day 21, the media were changed to RPMI 1640/B27 and changed every day. Finally, from day 22 to day 28, monolayer cells can be isolated into cell clusters and kept in low attachment for another week.

Statistics

Normal distribution and equal variance were confirmed before using the Student's *t*-test (two-tailed, unpaired) to estimate statistical significance. For contingency tables, we used Fisher's exact test. Statistical analysis was performed using Prism (GraphPad Software, La Jolla, CA).

Data availability

RNAseq and methylation data have been deposited in the GEO repository (https://www.ncbi.nlm.nih.gov/geo/) under accession number GEO SuperSeries GSE81571 and GSE86653.

Expanded View for this article is available online.

Acknowledgements
We thank María Guirola, Sheila Rueda, and the CNIO Histopathology Unit for technical support; Carmen Gómez and Patricia Prieto for help with iPSC/ESC culture; Zsuzsanna Izsvak (Max-Delbrück-Center for Molecular Medicine, Berlin, Germany) for reagents; Marta Cañamero (Pathology and Tissue Analytics, Roche Pharma, Basel, Switzerland) and Alba de Martino (Histopathology Unit, CNIO) for pathology advice; William Pu, Zhang-Peng Huang, and Kai Li (Cardiovascular Research Division, Boston Children's Hospital, USA) for help with the cardiac differentiation experiments; and Dr. Jennifer Franks (Geisel School of Medicine at Dartmouth, NH, USA) for her clarifications regarding the use of the FSQN method. We are indebted to the members of the CNIO Cell Division and Cancer laboratory for their constant support and advice. M.S.R. was supported by the Asociación Española contra el Cáncer (AECC; 2012 AIOA120833SALA and 2018 INVES18005SALA) and a Juan de la Cierva contract from the Ministry of Science, Innovation and Universities (MICIU). M.T. was supported by Fundación La Caixa. M.A.F. was supported by MICIU (SAF2014-60442-JIN). J.F.P. was funded by MICIU (RTI2018-093330-B/FEDER-EU), Ramón Areces Foundation (CIVP19S7917), CAM (B2017/BMD-3778), and AECC (2018, PROYE18054PIRI). F.V.M was supported by the National Breast Cancer Foundation/Cure Cancer Australia Foundation Postdoctoral Training Fellow. Work in S.J.C laboratory was supported by the National Health and Medical Research Council (NHMRC 1063560). M.A.B. laboratory is funded by SAF2013-45111-R from MICIU, Fundación Botín and Banco Santander, and Worldwide Cancer Research (WCR16-1177). Work in S.O. laboratory was funded by MICIU grant (SAF2013-44866-R). Work in the M.M. laboratory was supported by grants from the MICIU (RTI2018-095582-B-I00, RED2018-102723-T, and SAF2017-92729-EXP), and the iLUNG Programme (B2017/BMD-3884) from the Comunidad de Madrid. The CNIO is a Severo Ochoa Centers of Excellence (MICIU award SEV-2015-0510).

Author contributions
MS-R. performed most of the cellular and *in vivo* assays. MT contributed to the characterization of *mi*PSCs and MA-F and EZ-S to the generation of DNA constructs and molecular biology studies. FV-M, TJP, and SJC performed and analyzed the genome-wide methylation studies. CZ, YY, and JCI-B performed the human–mouse interspecies chimeric assays. OG-C analyzed RNAseq data. MA and MS participated in the evaluation of the data. MJB and MGC. generated the miR-203 knock-in mouse model, and JF-P contributed to its analysis. RS, MAB, and D-ZW contributed to the experiments of cardiomyocyte differentiation. JM and SO performed and analyzed tetraploid complementation assays, and SO supervised and analyzed embryo work. MS-R and MM conceived the project, supervised the work, and wrote the manuscript.

Conflict of interest
The authors declare that they have no conflict of interest.

References

Abad M, Mosteiro L, Pantoja C, Canamero M, Rayon T, Ors I, Grana O, Megias D, Dominguez O, Martinez D *et al* (2013) Reprogramming *in vivo* produces teratomas and iPS cells with totipotency features. *Nature* 502: 340 – 345

Bar-Nur O, Brumbaugh J, Verheul C, Apostolou E, Pruteanu-Malinici I, Walsh RM, Ramaswamy S, Hochedlinger K (2014) Small molecules facilitate rapid and synchronous iPSC generation. *Nat Methods* 11: 1170 – 1176

Beard C, Hochedlinger K, Plath K, Wutz A, Jaenisch R (2006) Efficient method to generate single-copy transgenic mice by site-specific integration in embryonic stem cells. *Genesis* 44: 23 – 28

Biase FH, Cao X, Zhong S (2014) Cell fate inclination within 2-cell and 4-cell mouse embryos revealed by single-cell RNA sequencing. *Genome Res* 24: 1787 – 1796

Blattler A, Yao L, Witt H, Guo Y, Nicolet CM, Berman BP, Farnham PJ (2014) Global loss of DNA methylation uncovers intronic enhancers in genes showing expression changes. *Genome Biol* 15: 469

Bock C, Reither S, Mikeska T, Paulsen M, Walter J, Lengauer T (2005) BiQ Analyzer: visualization and quality control for DNA methylation data from bisulfite sequencing. *Bioinformatics* 21: 4067 – 4068

Branco MR, Oda M, Reik W (2008) Safeguarding parental identity: Dnmt1 maintains imprints during epigenetic reprogramming in early embryogenesis. *Genes Dev* 22: 1567 – 1571

Bueno MJ, Perez de Castro I, Gomez de Cedron M, Santos J, Calin GA, Cigudosa JC, Croce CM, Fernandez-Piqueras J, Malumbres M (2008) Genetic and epigenetic silencing of microRNA-203 enhances ABL1 and BCR-ABL1 oncogene expression. *Cancer Cell* 13: 496 – 506

Burger L, Gaidatzis D, Schubeler D, Stadler MB (2013) Identification of active regulatory regions from DNA methylation data. *Nucleic Acids Res* 41: e155

Chen T, Ueda Y, Dodge JE, Wang Z, Li E (2003) Establishment and maintenance of genomic methylation patterns in mouse embryonic stem cells by Dnmt3a and Dnmt3b. *Mol Cell Biol* 23: 5594 – 5605

Chen J, Guo L, Zhang L, Wu H, Yang J, Liu H, Wang X, Hu X, Gu T, Zhou Z *et al* (2013) Vitamin C modulates TET1 function during somatic cell reprogramming. *Nat Genet* 45: 1504 – 1509

Choi J, Huebner AJ, Clement K, Walsh RM, Savol A, Lin K, Gu H, Di Stefano B, Brumbaugh J, Kim SY *et al* (2017a) Prolonged Mek1/2 suppression impairs the developmental potential of embryonic stem cells. *Nature* 548: 219 – 223

Choi YJ, Lin CP, Risso D, Chen S, Kim TA, Tan MH, Li JB, Wu Y, Chen C, Xuan Z *et al* (2017b) Deficiency of microRNA miR-34a expands cell fate potential in pluripotent stem cells. *Science* 355, eaag1927

Chung HC, Lin RC, Logan GJ, Alexander IE, Sachdev PS, Sidhu KS (2012) Human induced pluripotent stem cells derived under feeder-free conditions display unique cell cycle and DNA replication gene profiles. *Stem Cells Dev* 21: 206 – 216

Eckersley-Maslin M, Alda-Catalinas C, Blotenburg M, Kreibich E, Krueger C, Reik W (2019) Dppa2 and Dppa4 directly regulate the Dux-driven zygotic transcriptional program. *Genes Dev* 33: 194 – 208

Feng H, Conneely KN, Wu H (2014) A Bayesian hierarchical model to detect differentially methylated loci from single nucleotide resolution sequencing data. *Nucleic Acids Res* 42: e69

Franks JM, Cai G, Whitfield ML (2018) Feature specific quantile normalization enables cross-platform classification of molecular subtypes using gene expression data. *Bioinformatics* 11: 1868 – 1874

Gasque Schoof CR, Izzotti A, Jasiulionis MG, Vasques Ldos R (2015) The roles of miR-26, miR-29, and miR-203 in the silencing of the epigenetic machinery during melanocyte transformation. *Biomed Res Int* 2015: 634749

Goossens K, Mestdagh P, Lefever S, Van Poucke M, Van Zeveren A, Van Soom A, Vandesompele J, Peelman L (2013) Regulatory microRNA network identification in bovine blastocyst development. *Stem Cells Dev* 22: 1907 – 1920

Graña O, Rubio-Camarillo M, Fernandez-Riverola F, Pisano SG, Gonzalez-Peña D (2018) nextpresso: next generation sequencing expression analysis pipeline. *Curr Bioinformatics* 13: 583 – 591

Hirasawa R, Chiba H, Kaneda M, Tajima S, Li E, Jaenisch R, Sasaki H (2008) Maternal and zygotic Dnmt1 are necessary and sufficient for the maintenance of DNA methylation imprints during preimplantation development. *Genes Dev* 22: 1607 – 1616

Huang ZP, Kataoka M, Chen J, Wu G, Ding J, Nie M, Lin Z, Liu J, Hu X, Ma L *et al* (2015) Cardiomyocyte-enriched protein CIP protects against pathophysiological stresses and regulates cardiac homeostasis. *J Clin Invest* 125: 4122 – 4134

Jackson M, Krassowska A, Gilbert N, Chevassut T, Forrester L, Ansell J, Ramsahoye B (2004) Severe global DNA hypomethylation blocks differentiation and induces histone hyperacetylation in embryonic stem cells. *Mol Cell Biol* 24: 8862 – 8871

Kang L, Wang J, Zhang Y, Kou Z, Gao S (2009) iPS cells can support full-term development of tetraploid blastocyst-complemented embryos. *Cell Stem Cell* 5: 135 – 138

Kattman SJ, Witty AD, Gagliardi M, Dubois NC, Niapour M, Hotta A, Ellis J, Keller G (2011) Stage-specific optimization of activin/nodal and BMP signaling promotes cardiac differentiation of mouse and human pluripotent stem cell lines. *Cell Stem Cell* 8: 228 – 240

Langmead B, Trapnell C, Pop M, Salzberg SL (2009) Ultrafast and memory-efficient alignment of short DNA sequences to the human genome. *Genome Biol* 10: R25

Latos PA, Sienerth AR, Murray A, Senner CE, Muto M, Ikawa M, Oxley D, Burge S, Cox BJ, Hemberger M (2015) Elf5-centered transcription factor hub controls trophoblast stem cell self-renewal and differentiation through stoichiometry-sensitive shifts in target gene networks. *Genes Dev* 29: 2435 – 2448

Lee HJ, Hinshelwood RA, Bouras T, Gallego-Ortega D, Valdes-Mora F, Blazek K, Visvader JE, Clark SJ, Ormandy CJ (2011) Lineage specific methylation of the Elf5 promoter in mammary epithelial cells. *Stem Cells* 29: 1611 – 1619

Leitch HG, McEwen KR, Turp A, Encheva V, Carroll T, Grabole N, Mansfield W, Nashun B, Knezovich JG, Smith A *et al* (2013) Naive pluripotency is associated with global DNA hypomethylation. *Nat Struct Mol Biol* 20: 311 – 316

Li H, Durbin R (2009) Fast and accurate short read alignment with Burrows-Wheeler transform. *Bioinformatics* 25: 1754 – 1760

Li Y, Zhang Q, Yin X, Yang W, Du Y, Hou P, Ge J, Liu C, Zhang W, Zhang X *et al* (2011) Generation of iPSCs from mouse fibroblasts with a single gene, Oct4, and small molecules. *Cell Res* 21: 196 – 204

Li M, Izpisua Belmonte JC (2016) Looking to the future following 10 years of induced pluripotent stem cell technologies. *Nat Protoc* 11: 1579 – 1585

Liao J, Karnik R, Gu H, Ziller MJ, Clement K, Tsankov AM, Akopian V, Gifford CA, Donaghey J, Galonska C *et al* (2015) Targeted disruption of DNMT1, DNMT3A and DNMT3B in human embryonic stem cells. *Nat Genet* 47: 469 – 478

Lister R, Pelizzola M, Dowen RH, Hawkins RD, Hon G, Tonti-Filippini J, Nery JR, Lee L, Ye Z, Ngo QM *et al* (2009) Human DNA methylomes at base resolution show widespread epigenomic differences. *Nature* 462: 315 – 322

Liu Y, Siegmund KD, Laird PW, Berman BP (2012) Bis-SNP: combined DNA methylation and SNP calling for Bisulfite-seq data. *Genome Biol* 13: R61

MacFarlan TS, Gifford W, Driscoll S, Lettieri K, Rowe H, Bonanomi D, Firth A, Singer O, Trono D, Pfaff SL (2012) ES cell potency fluctuates with endogenous retrovirus activity. *Nature* 487: 57 – 63

Martin M (2011) Cutadapt removes adapter sequences from high-throughput sequencing reads. *EMBnet J* 17: 10 – 12

Mascetti VL, Pedersen RA (2016) Human-mouse chimerism validates human stem cell pluripotency. *Cell Stem Cell* 18: 67 – 72

Michel CI, Malumbres M (2013) microRNA-203: tumor suppression and beyond. *MicroRNA* 2: 118 – 126

Mikkelsen TS, Hanna J, Zhang X, Ku M, Wernig M, Schorderet P, Bernstein BE, Jaenisch R, Lander ES, Meissner A (2008) Dissecting direct reprogramming through integrative genomic analysis. *Nature* 454: 49 – 55

Miyata S, Minobe W, Bristow MR, Leinwand LA (2000) Myosin heavy chain isoform expression in the failing and nonfailing human heart. *Circ Res* 86: 386 – 390

Najm FJ, Chenoweth JG, Anderson PD, Nadeau JH, Redline RW, McKay RD, Tesar PJ (2011) Isolation of epiblast stem cells from preimplantation mouse embryos. *Cell Stem Cell* 8: 318 – 325

Okano M, Bell DW, Haber DA, Li E (1999) DNA methyltransferases Dnmt3a and Dnmt3b are essential for *de novo* methylation and mammalian development. *Cell* 99: 247 – 257

Okita K, Ichisaka T, Yamanaka S (2007) Generation of germline-competent induced pluripotent stem cells. *Nature* 448: 313 – 317

Otsuji TG, Minami I, Kurose Y, Yamauchi K, Tada M, Nakatsuji N (2010) Progressive maturation in contracting cardiomyocytes derived from human embryonic stem cells: qualitative effects on electrophysiological responses to drugs. *Stem Cell Res* 4: 201 – 213

Pedersen BS, Eyring K, De S, Yang IV, Schwartz DA (2014) Fast and accurate alignment of long bisulfite-seq reads. *arxiv* https://arxiv.org/abs/1401.1129 [PREPRINT]

Peters TJ, Buckley MJ, Statham AL, Pidsley R, Samaras K, Lord RV, Clark SJ, Molloy PL (2015) *De novo* identification of differentially methylated regions in the human genome. *Epigenet Chrom* 8: 6

Rosenbloom KR, Armstrong J, Barber GP, Casper J, Clawson H, Diekhans M, Dreszer TR, Fujita PA, Guruvadoo L, Haeussler M *et al* (2015) The UCSC genome browser database: 2015 update. *Nucleic Acids Res* 43: D670 – D681

Sandhu R, Rivenbark AG, Coleman WB (2012) Loss of post-transcriptional regulation of DNMT3b by microRNAs: a possible molecular mechanism for the hypermethylation defect observed in a subset of breast cancer cell lines. *Int J Oncol* 41: 721 – 732

Takahashi K, Yamanaka S (2006) Induction of pluripotent stem cells from mouse embryonic and adult fibroblast cultures by defined factors. *Cell* 126: 663 – 676

Stadtfeld M, Apostolou E, Akutsu H, Fukuda A, Follett P, Natesan S, Kono T, Shioda T, Hochedlinger K (2010a) Aberrant silencing of imprinted genes on chromosome 12qF1 in mouse induced pluripotent stem cells. *Nature* 465: 175 – 181

Stadtfeld M, Maherali N, Borkent M, Hochedlinger K (2010b) A reprogrammable mouse strain from gene-targeted embryonic stem cells. *Nat Methods* 7: 53 – 55

Takahashi K, Yamanaka S (2016) A decade of transcription factor-mediated reprogramming to pluripotency. *Nat Rev Mol Cell Biol* 17: 183 – 193

Theunissen TW, Friedli M, He Y, Planet E, O'Neil RC, Markoulaki S, Pontis J, Wang H, Iouranova A, Imbeault M *et al* (2016) Molecular criteria for defining the naive human pluripotent state. *Cell Stem Cell* 19: 502 – 515

To KK, Leung WW, Ng SS (2017) A novel miR-203-DNMT3b-ABCG2 regulatory pathway predisposing colorectal cancer development. *Mol Carcinog* 56: 464 – 477

Trapnell C, Roberts A, Goff L, Pertea G, Kim D, Kelley DR, Pimentel H, Salzberg SL, Rinn JL, Pachter L (2012) Differential gene and transcript expression analysis of RNA-seq experiments with TopHat and Cufflinks. *Nat Protoc* 7: 562 – 578

Wang Y, Gao S (2016) Human naïve embryonic stem cells: how full is the glass? *Cell Stem Cell* 18: 301 – 303

Wu J, Greely HT, Jaenisch R, Nakauchi H, Rossant J, Belmonte JC (2016) Stem cells and interspecies chimaeras. *Nature* 540: 51 – 59

Xie W, Schultz MD, Lister R, Hou Z, Rajagopal N, Ray P, Whitaker JW, Tian S, Hawkins RD, Leung D *et al* (2013) Epigenomic analysis of multilineage differentiation of human embryonic stem cells. *Cell* 153: 1134 – 1148

Yagi M, Kishigami S, Tanaka A, Semi K, Mizutani E, Wakayama S, Wakayama T, Yamamoto T, Yamada Y (2017) Derivation of ground-state female ES cells maintaining gamete-derived DNA methylation. *Nature* 548: 224 – 227

Yang Y, Bai W, Zhang L, Yin G, Wang X, Wang J, Zhao H, Han Y, Yao YQ (2008) Determination of microRNAs in mouse preimplantation embryos by microarray. *Dev Dyn* 237: 2315 – 2327

Yang Y, Liu B, Xu J, Wang J, Wu J, Shi C, Xu Y, Dong J, Wang C, Lai W *et al* (2017) Derivation of pluripotent stem cells with *in vivo* embryonic and extraembryonic potency. *Cell* 169: 243 – 257 e25

Yi R, Poy MN, Stoffel M, Fuchs E (2008) A skin microRNA promotes differentiation by repressing "stemness". *Nature* 452: 225 – 229

Ying QL, Wray J, Nichols J, Batlle-Morera L, Doble B, Woodgett J, Cohen P, Smith A (2008) The ground state of embryonic stem cell self-renewal. *Nature* 453: 519 – 523

Zhao XY, Li W, Lv Z, Liu L, Tong M, Hai T, Hao J, Guo CL, Ma QW, Wang L *et al* (2009) iPS cells produce viable mice through tetraploid complementation. *Nature* 461: 86 – 90

